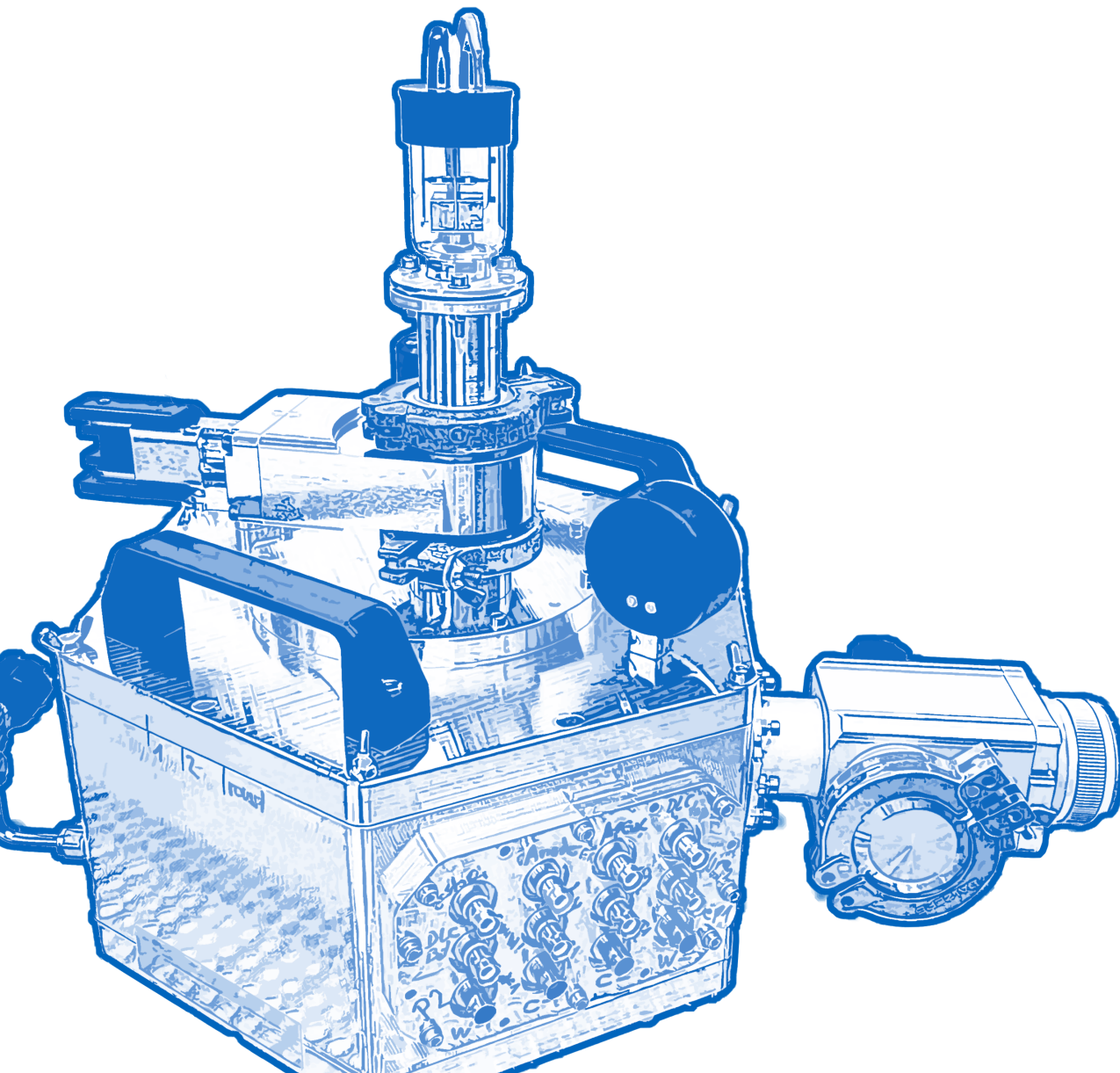


Bachelor's thesis

# Characterizing CsI Coated THGEMs for Photon Detection

Markus Rieder





TECHNICAL UNIVERSITY MUNICH

BACHELOR'S THESIS  
PHYSICS

# Characterizing CsI Coated THGEMs for Photon Detection

## Charakterisierung von CsI beschichteten THGEMs für Photonendetektion

MARKUS RIEDER



**Supervisor:** Prof. Dr. Laura Fabbietti  
**Advisor:** Thomas Klemenz  
**Date:** 29.08.2022

# AUTHORSHIP

With my signature I confirm that this bachelor's thesis "Characterizing CsI coated THGEMs for photon detection" is my own work and I have documented all sources and materials used.

Mit meiner Unterschrift versichere ich, dass ich die von mir eingereichte Bachelorarbeit "Charakterisierung von CsI beschichteten THGEMs für Photonendetektion" alleine verfasst habe und keine anderen als die angegebenen Quellen und Hilfsmittel benutzt habe.

Munich, 29.08.2022



---

Ort, Datum

Unterschrift

# ABSTRACT

Photodetectors capable of single photon detection in the visible wavelength region are relevant in many parts of modern physics, especially in the field of neutrino-physics. There is an ongoing effort for using THGEMs for photon detection, as these can provide more cost-effective scalability to large areas than currently deployed photodetectors (e.g. PMTs).

In this bachelor's thesis the properties of CsI coated THGEMs were investigated. Initially measurements were performed to understand the movement of photoelectrons inside the detector vessel, both in vacuum and in gas. After this the focus was placed on the properties of the photocathode material, which largely determines the quality and performance of THGEM based photodetectors. For this thesis THGEMs were coated with a layer of CsI at a clean room facility at the TUM. The quantum efficiency of this photocathode and its decline due to gas exposure and ion bombardment was measured. A quantum efficiency value of 7.74% at a wavelength of  $\lambda = 161 \text{ nm}$  for a reflective CsI photocathode is reported. No decline in quantum efficiency after long exposure to Ar-CH<sub>4</sub> (90-10), but a decrease in quantum efficiency of 50% after a charge deposition of around  $50 \mu\text{C}/\text{mm}^2\text{s}$  on the photocathode was recorded. The last aspect of this research was to determine the maximum gain that could be reached with our single THGEM setup in Ar-CH<sub>4</sub> (90-10). These measurements were performed with an uncoated and a CsI coated THGEM. In both cases a gain of around  $1.2 \cdot 10^3$  was attained, before discharges started occurring.

# Contents

<b>1</b>	<b>Introduction</b>	<b>4</b>
1.1	Properties of (TH)GEMs . . . . .	5
1.2	Working principle of (TH)GEMs . . . . .	6
1.3	THGEMs for photon detection . . . . .	7
<b>2</b>	<b>Experiment</b>	<b>9</b>
2.1	The detector . . . . .	9
2.2	Coating procedure . . . . .	13
2.3	Methodology . . . . .	14
2.3.1	Gain . . . . .	15
2.3.2	Quantum efficiency . . . . .	16
2.3.3	Aging . . . . .	19
<b>3</b>	<b>Results and discussion</b>	<b>20</b>
3.1	E-to-wires measurement . . . . .	20
3.1.1	In vacuum . . . . .	20
3.1.2	In gas . . . . .	23
3.2	Gain measurement . . . . .	25
3.2.1	Linear fitting to plateau . . . . .	26
3.2.2	E-to-wires measurement . . . . .	26
3.2.3	$I_{prim}$ of CsI coated and uncoated Au THGEM . . . . .	29
3.2.4	Gain of CsI coated and uncoated Au THGEM . . . . .	30
3.3	Quantum efficiency of CsI PC . . . . .	32
3.3.1	Diode reference measurement . . . . .	33
3.3.2	QE calculation . . . . .	33
3.3.3	Comparison to DLC GEM . . . . .	34
3.4	Aging studies . . . . .	35
3.4.1	Exposure to gas . . . . .	35
3.4.2	Ion bombardment . . . . .	36
<b>4</b>	<b>Summary and outlook</b>	<b>39</b>
<b>5</b>	<b>Appendix</b>	<b>44</b>
<b>6</b>	<b>Acknowledgements</b>	<b>49</b>
	<b>References</b>	<b>50</b>

# 1 Introduction

Neutrinos are neutral fermions with a very small mass and interact with matter via the weak interaction. They were first postulated in the 1930s and the first neutrino flavor to be experimentally discovered was the electron antineutrino with an experiment using a bubble chamber in 1956 [1]. Since then a multitude of experiments has shed more light on the field of neutrino physics and answered many outstanding questions while also raising many new ones. This field is constantly changing and with it, the requirements modern detectors need to fulfill to push the boundaries of our current understanding.

As times have changed, so have the type of detectors used for experiments concerning neutrino physics. With that being said, most of the modern experiments, which have led to milestone discoveries in this field, like the Super-Kamiokande [2] or the IceCube neutrino observatory [3], are detectors that have a very similar setup. For one, these detectors are massive in size. The reason is, that while neutrinos are abundant in the universe and billions pass through us every second, they rarely interact with matter. Therefore to get a sufficient amount of data from these rare interactions, the detectors must observe large areas. Another similarity between these detectors is the use of a large number of photodetectors. This stems from the problem, that neutrinos can only be measured indirectly. The most common way of doing this is by observing the Cherenkov light from charged particles, which interacted with a neutrino. This Cherenkov light cone is emitted, when a charged particle travels through a medium at a speed greater than the phase velocity of light in that medium.

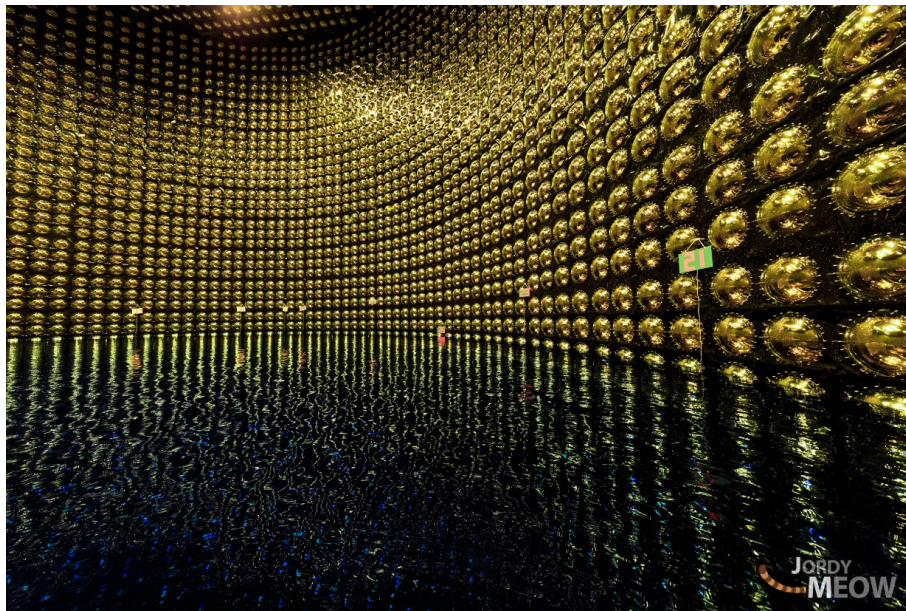


Figure 1: The inside of the Super-Kamiokande detector, which is surrounded by thousands of photomultiplier tubes. Credit: Jordy Meow [4].

Now one might think, as the experiments increase in size, the photodetectors should do the same to keep up with the requirements. The problem with the type

of photodetector commonly used in these experiments, which is the photomultiplier tube (PMT), is, that the design requires PMTs to be quite compact [5]. In other words, the larger the area to be observed gets, the more PMTs have to be installed. For example, Super-Kamiokande has a detector volume filled with 50kt of ultra-pure water, which is surrounded by about 11200 PMTs [6]. Not only is this quite expensive, but it also begs the question if there isn't a better-suited type of photodetector, that can be used for detecting light in the visible wavelength range and also has the potential for large-scale application. These are the requirements that set the stage for researching THGEMs as photodetectors.

### 1.1 Properties of (TH)GEMs

First the basic features of (TH)GEMs must be discussed. In 1997 Fabio Sauli developed a new type of micropattern gaseous detector (MPGD), called GEM, short for gas electron multiplier, to be used for the detection of ionizing particles [7]. The design of a GEM incorporates a Kapton foil, 50 – 70  $\mu\text{m}$  thick, with copper coating on both sides, which is perforated with tiny holes. These holes are chemically etched into the material and have a diameter of 70  $\mu\text{m}$  and a hole pitch of 140  $\mu\text{m}$  [8].

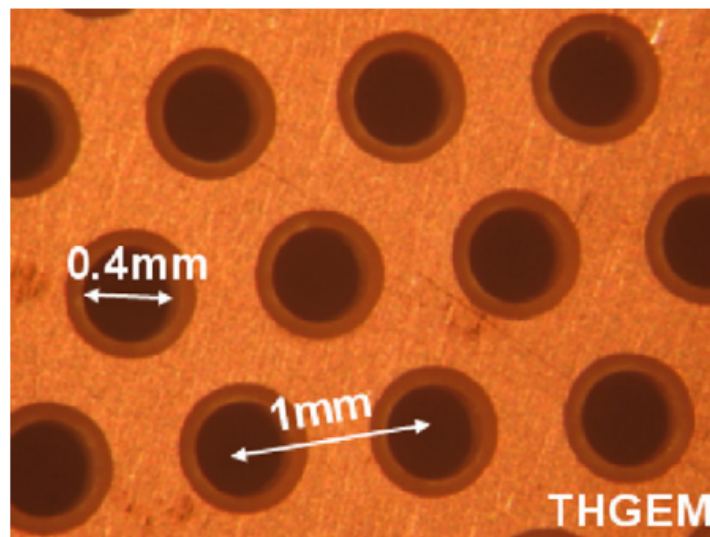


Figure 2: Dimensions of a standard THGEM.[9]

THGEMs, Thick gas electron multipliers, are, as the name suggests, GEMs with larger dimensions and were first introduced by Checknik et al [10]. Instead of using Kapton foil, THGEMs are usually made out of 500  $\mu\text{m}$  thick PCB material. The holes, which are mechanically drilled, have a diameter of 400  $\mu\text{m}$  with a 800  $\mu\text{m}$  pitch, see figure 2. The larger dimension make THGEMs easier and cheaper to manufacture and also more mechanically robust compared to GEMs.

## 1.2 Working principle of (TH)GEMs

The operational principle of (TH)GEMs consists of applying a potential difference between the top and bottom side of the (TH)GEM, which leads to an electric field in and in close proximity around the holes. Figure 3 depicts a simulation of the above-mentioned resulting electric dipole field.

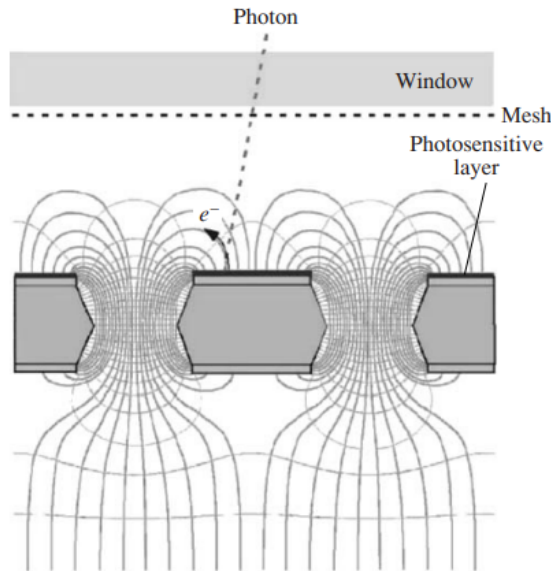


Figure 3: The electric field in and around a GEM covered with a photosensitive layer is shown in this picture. [11].

Detectors utilizing (TH)GEMs are filled with gas. If an electron gets guided into the hole and gets accelerated due to the strong electric field, it can ionize gas atoms, leading to a multitude of free electrons. This effect is described as an electron avalanche. The amount of free electrons produced in the hole depends on the strength of the electric field in the hole. The stronger the electric field, the faster the electrons achieve ionization energies, which leads to a higher number of ionized gas atoms. This also depends on the gas being used, as each gas has unique ionization energies.

(TH)GEMs, as mentioned above, were first conceived to be used as ionizing particle detectors. In this case, the initial electrons entering the holes are created, when ionizing radiation creates free electrons in the gas volume. These electrons are then guided to the holes of the (TH)GEM with the use of an electric field, where they initiate an electron avalanche and therefore create enough electrons to produce a current, which is detectable with read-out electronics. This application of (TH)GEMs can be seen on the right side of figure 4. One of the limiting factors of (TH)GEMs is, that when gas atoms are ionized in the hole, it not only leads to free electrons but also an equivalent number of ions inside the hole. At high enough potential differences the number of electrons and ions result in a change of the electric field inside the hole, which can lead to a spark across the (TH)GEM. These discharges can damage the detector and lead to a significant loss in performance.

But apart from using (TH)GEMs as ionizing particle detectors, they can also be used as photodetectors.

### 1.3 THGEMs for photon detection

To use THGEMs as a photodetector for photons, that do not have enough energy to ionize gas particles, one has to find a way to convert the photons into electrons. This is achieved by taking advantage of the photo effect, first postulated by Albert Einstein in 1905, which describes the process of a material emitting an electron when an electromagnetic wave hits it [12]. Experiments performed during that time showed, that the emission of electrons doesn't depend on the intensity, but rather on the frequency of the used light source. Einstein postulated that light is made out of discrete energy packets called photons. This for its time revolutionary concept of photons leads to a simple equation, which describes the photoeffect:

$$E_{kinetic} = h \cdot f - W \quad (1)$$

The left side of the equation corresponds to the kinetic energy of the emitted electrons and the right side explains how this depends on the energy of the photon,  $E = h \cdot f$ , and on the work-function  $W$  of the material. The energy of the photon depends on the frequency  $f$  of the light source. It is this relationship that is imperative to understand when talking about THGEMs for photon detection because in order to convert photons into electrons one must combine THGEMs with a photocathode (PC). There are two ways of doing this, both portrayed in figure 4.

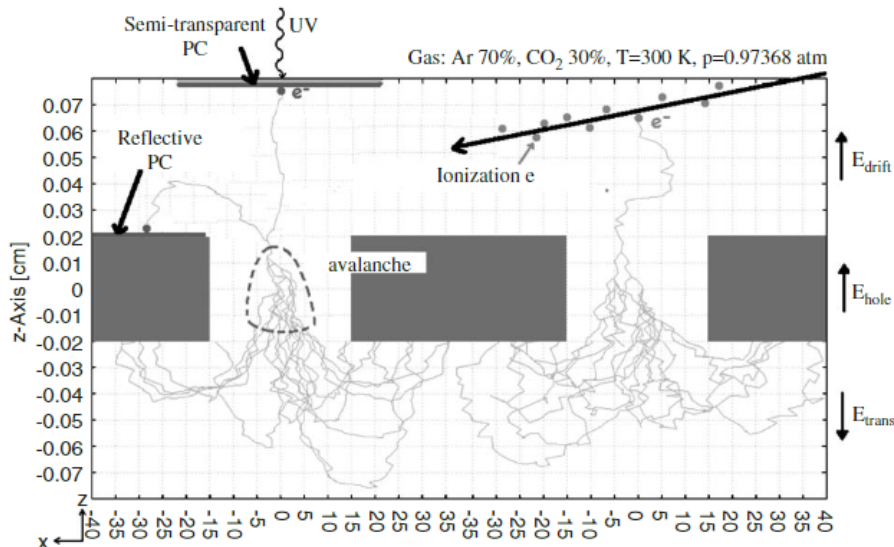


Figure 4: This picture illustrates different applications for THGEMs: As a ionizing particle detector or a photodetector with a reflective or a semitransparent PC [13]

In the case of the semitransparent PC, the entrance window of the photodetector is coated with the PC. If photoelectrons are emitted they drift to the THGEM

due to an electric field and then get multiplied inside the THGEM hole. The semi-transparent PC is pictured in the top left of figure 4. This setup has some drawbacks, for example, the photon feedback to the PC due to avalanche scintillation [11]. Reflective PCs on the other hand are coated directly onto the top side of the THGEM. If a photon hits the PC and a photoelectron is emitted, it will get guided into a hole by the dipole field of the THGEM, see figure 3, and undergo avalanche amplification. In this bachelor's thesis, a reflective Caesium iodide (CsI) PC and a single THGEM setup were used.

There are a couple of experiments that already successfully operate (TH)GEM based photodetectors, for example, the HADES RICH detector [14]. There are two main considerations to be made before applying THGEMs as photodetectors. The first one depends on the quality and longevity of the PC material, as this impacts the detector's ability to measure photons. The second consideration is the gain the setup can reach while ensuring stable operation of the detector.

In this bachelor's thesis, these properties are explained, measured, and discussed to characterize the performance of CsI coated THGEMs for photodetection.

## 2 Experiment

### 2.1 The detector

The detector vessel used throughout the tenure of this bachelor's thesis is made out of aluminium and has a volume of around 7 liters. It is pictured in figure 5.

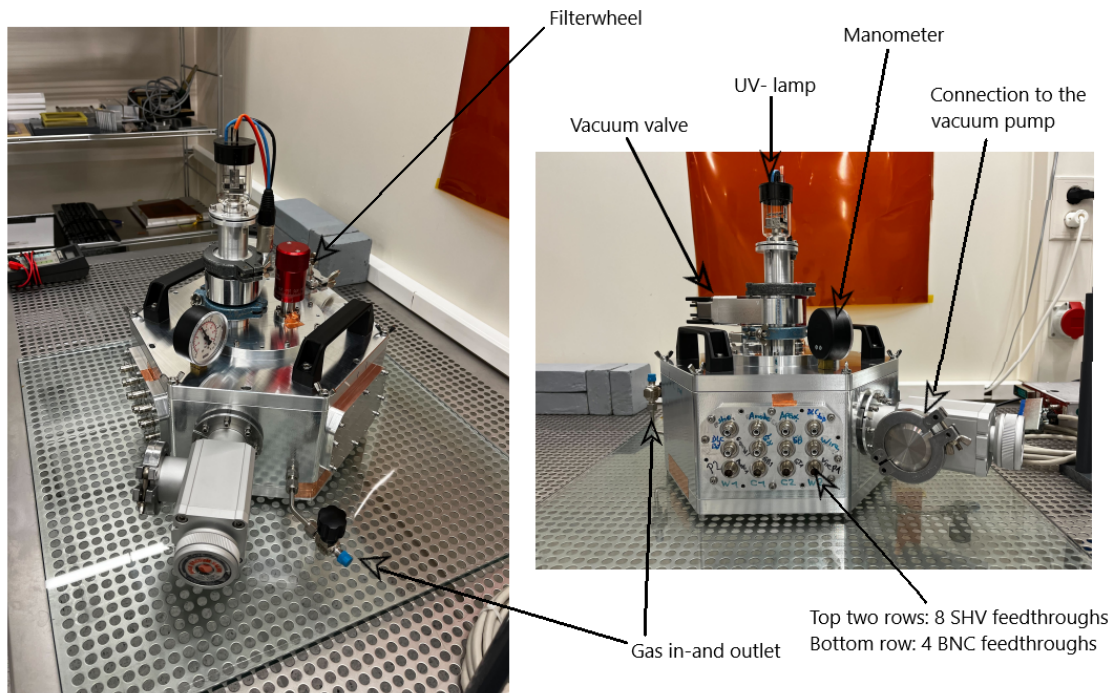


Figure 5: This is the detector vessel used during the experiment. These pictures depict the detector in a clean room environment and not in operational mode.

The basic elements of this setup include a manometer (WIKA Typ 111.10), 8 SHV feedthroughs, 4 BNC feedthroughs, a filter wheel (Pfeiffer Vacuum Magnetically coupled rotary union) - all filters are listed in table 4 -, a Deuterium lamp (Cathodeon Type No. V03) with a built-in  $\text{MgF}_2$  window and a vacuum valve, to shield the detector from any light.

To operate the detector and take measurements the following devices are used: A high voltage power supply module (iseg ECH 224), a picoammeter (Pico Logic PA 125-24) - which has an upper limit for current values of 130 nA -, an electrometer (Keithley 6517B), a vacuum pump (Pfeiffer vacuum pump TSH 071) and a lamp power supply (Cathodeon LTD deuterium lamp supply C711) to operate the UV-lamp. With the vacuum pump pressure values of around  $p = 4 \cdot 10^{-6}$  mbar can be reached. When performing gas measurements, which are done in  $\text{Ar}-\text{CH}_4$  (mixture: 90-10), the flow of the gas is regulated with a flow meter (Voegtlin Typ V-100) and set to 10 liters per hour. The currents are recorded with a *LabVIEW* program, which also calculates the standard deviation.

## 2.1 The detector

The experimental setup in the laboratory is pictured in figure 6 and figure 7.

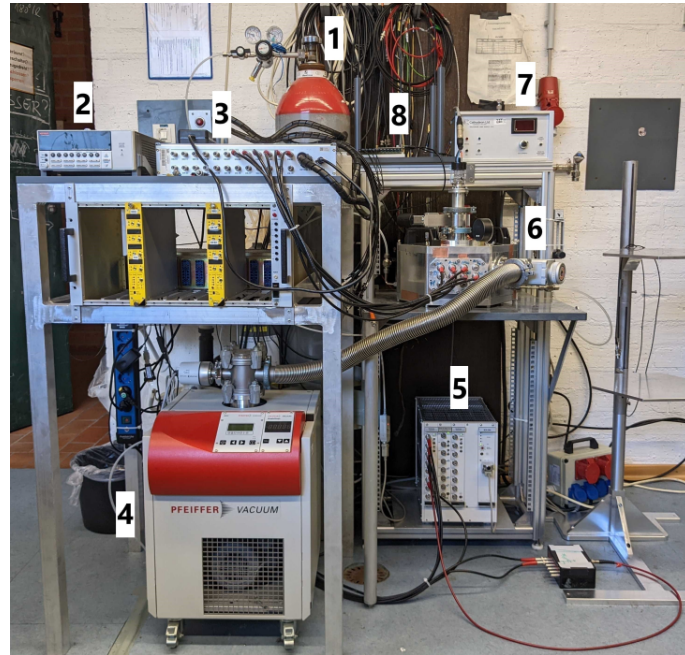


Figure 6: This is the operational setup. (1) shows the gas bottle filled with Ar-CH<sub>4</sub> in a 90-10 mixture. (2) shows the Keithley electrometer and (3) the pA-meter. (4) shows the vacuum pump and (5) the high voltage supply. (6) shows the detector vessel and (7) the Cathodeon lamp power supply. Lastly (8) shows the FPGA board (Cyclone 4 -USB 2.0).

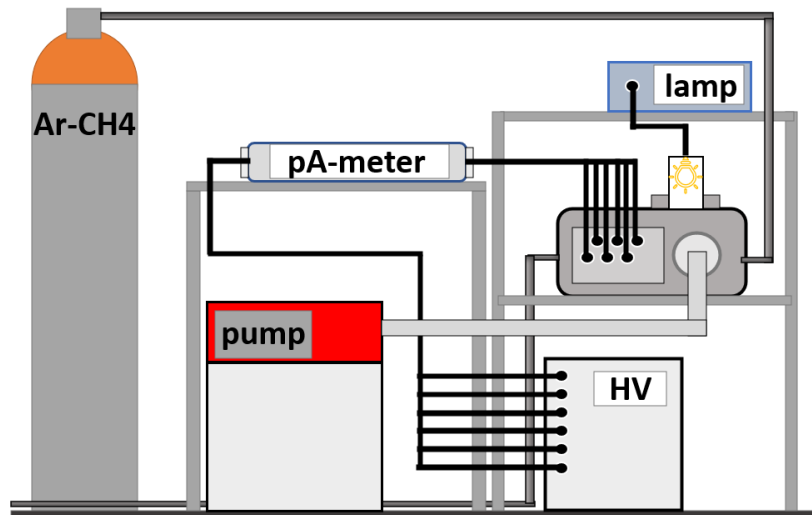


Figure 7: This is a sketch of the operational setup. All connections from and to the detector vessel are shown.

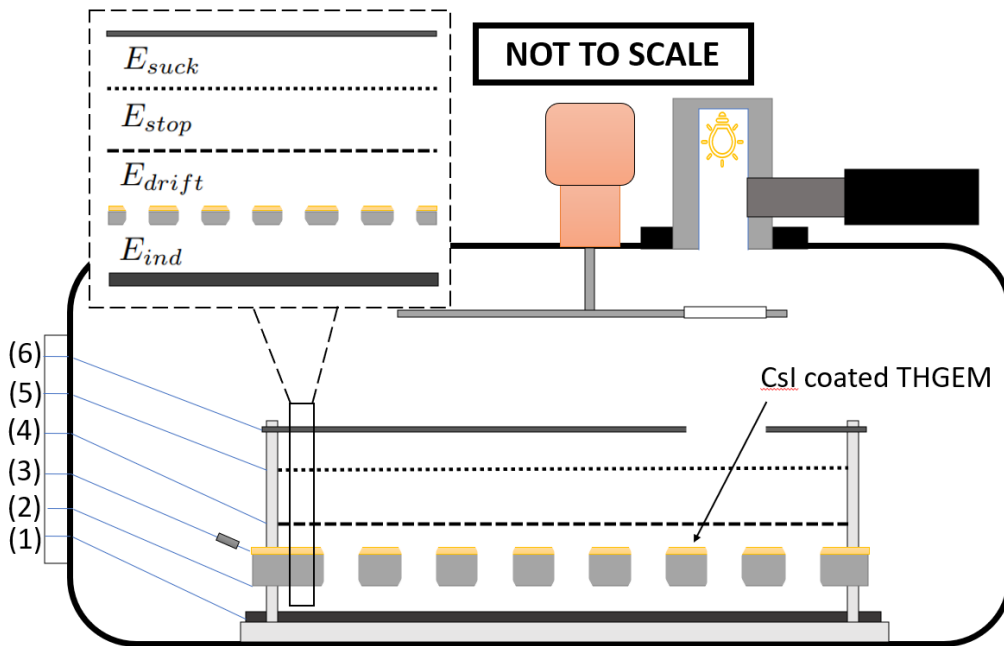


Figure 8: This sketch shows the cross section of the detector vessel. The Deuterium lamp, the vacuum valve, the filter wheel and the electrodes are depicted. The current measured and voltage supplied at each electrode (1)-(6) is shown. The electric field between each electrode is shown as (7)-(10). The variable names assigned to each number in the figure are documented in table 1.

Figure 8 shows a sketch of the inside of the detector vessel. It is important to note that the provided sketch shows a uniform CsI coating across the THGEM, which in reality is not the case and will be discussed in the next section. The black handle on the right side of the lamp is a vacuum valve used to block the light of the UV-lamp from entering the detector vessel.

The electrodes are kept in place by eight Teflon pins, which are mounted to a baseplate made out of Delrin and fixed to the bottom of the detector. The electrodes are kept at a fixed distance  $d$  from each other with the use of Teflon spacers. Naming these electrodes from order bottom to top: anode, THGEM bottom, THGEM top, wires, mesh and aperture.

The aperture is made out of aluminium. It has a round hole directly beneath the lamp, as this restricts the active area being illuminated by the light source. Therefore QE calculations, which are explained later, are more precise because the number of photons can be determined with a higher degree of certainty. The diameter of the hole is 20 mm. The aperture is sandblasted on the side facing the lamp. A smooth surface would result in some photons being reflected off the aperture back to the filters. From there, photons could reflect and go through the hole of the aperture, which would alter the amount of photons hitting the illuminated area of the PC. The sandblasting reduces this effect. The mesh - made out of stainless steel- and wires - made out of Tungsten - have a combined transparency of around 51%.

Each electrode is connected with cables the same way to the voltage power sup-

ply via one of the eight SHV feedthroughs, with one exception being THGEM top, as a resistor ( $\approx 5 \text{ M}\Omega$ ) is additionally put in place to shield the picoammeter (pA-meter) from discharge currents.

The applied voltage to each electrode and the variable names for the measured current, which will be used throughout this thesis, are listed in the left table 1 next to the table containing the variable names of the electric fields between the electrodes.

electrode	current	voltage
(1) anode	$I_{anode}$	$U_{anode}$
(2) $THGEM_{bot}$	$I_{GB}$	$U_{GB}$
(3) $THGEM_{top}$	$I_{GT}$	$U_{GT}$
(4) wires	$I_{wires}$	$U_{wires}$
(5) mesh	$I_{stop}$	$U_{mesh}$
(6) aperture	$I_{suck}$	$U_{aperture}$

Between electrodes	electric field
anode and THGEM bot	$E_{ind}$
THGEM top and wires	$E_{drift}$
wires and mesh	$E_{stop}$
mesh and aperture	$E_{suck}$

Table 1: *Left table:* This table documents the variable name, the measured currents and the supplied voltage of each electrode. *Right table:* This table documents the variable names of the electric field between the respective electrodes and indicates between which electrode which electric field exists. All numbers are in accordance to the sketch in figure 8.

The formula to calculate these electric fields,  $E = \Delta U/d$ , depends on the potential difference  $\Delta U$  and the distance  $d$  between the electrodes, which are listed in table 3.

electrode material	workfunction eV
Aluminium	$\approx 4.2$
Tungsten	$\approx 4.9$
Stainless steel	$\approx 4.4$

Table 2: Work functions of electrode material. The work functions depend heavily on gas and preparation, but these values should give an indication if photo electrons can be emitted by photons of the UV-lamp.[15] [16]

electrodes	distance [mm]
anode to mesh	2
mesh to wires	3
wires to THGEM top	3.6
THGEM bot to anode	2

Table 3: The distance  $d$  between the individual electrodes is shown.

A potential difference between the top and bottom side of the THGEM, called  $\Delta U_{THGEM}$ , leads to an electric field in and around the holes of the THGEM, as can be seen in figure 3.

## 2.2 Coating procedure

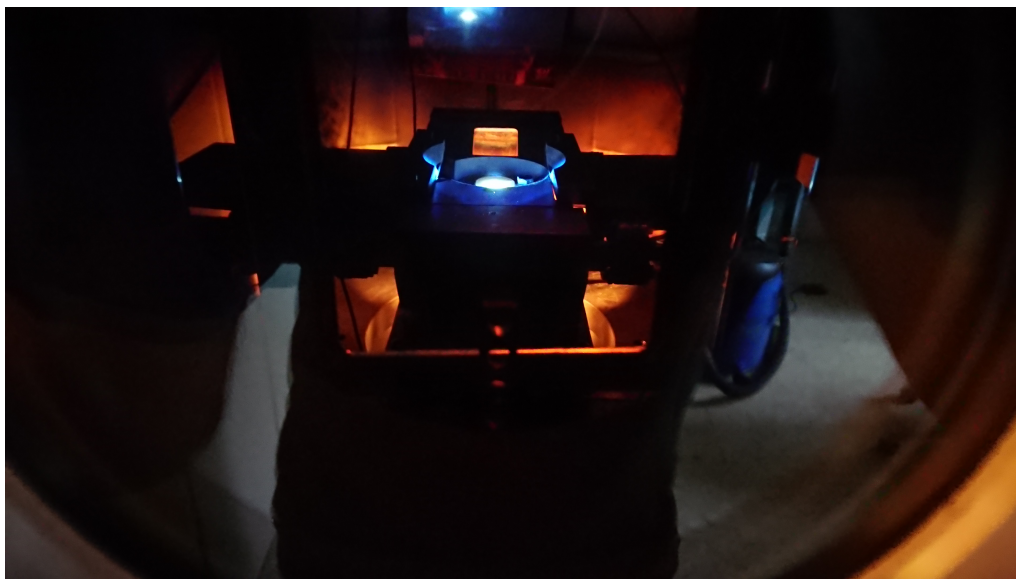


Figure 9: This picture was taken during the coating process. The CsI is heated and evaporated onto sections of the uncoated THGEM. The blue circle in the middle of the picture is the used CsI pill.

The THGEMs are coated with Caesium iodide (CsI) at a clean room facility in the physics department at the TUM. The THGEMs used during this bachelor's thesis have a total area of  $180 \times 180 \text{ mm}^2$ , are made out of a  $500 \mu\text{m}$  thick PCB material called FR4 and are coated on both sides with a  $5 \mu\text{m}$  thick Au layer.

The active area of the THGEM, which is the Au coated area perforated with holes, is  $A = 113 \times 113 \text{ mm}^2$  and is sectioned into three segments, each  $37.5 \text{ mm}$  wide. The hole to surface ratio is 0.2267. After coating the THGEM, it is built into the detector vessel. Exposure to air is known to be a major contributor to the decline in performance for solid PCs [11], therefore limiting the time the freshly coated THGEM spends outside the detector vessel is important.

The coating process involves having the uncoated THGEM in a high vacuum environment and depositing the CsI onto it via electron beam evaporation, which can be seen in figure 9. As mentioned above, not the whole area of the THGEM is coated but rather two areas, as can be seen in figure 10. The area of the PC is  $A = 2 \times 4 \text{ cm}^2$  per coated section. The exact coating procedure and coating facility at the TUM are explained in detail in papers concerning the coating of the HADES RICH mirrors, see [17]. Heat treatment after coating, which have been shown to increase the quality of the PC [11], were not performed.

Two CsI coated THGEMs are used during this bachelor's thesis. The first coated THGEM has a CsI PC that is  $195 \text{ nm}$  thick and is used primarily for experiments conducted to understand the electron movement inside our detector vessel.

The second CsI PC is  $205 \text{ nm}$  thick and is used for aging measurements. The marginal difference in the thickness of the coating should not impact the QE of

## 2.3 Methodology

the individual PC [18]. It should be mentioned, that the first PC was coated in early March, while the second PC was coated in July, when the humidity was higher. As CsI is strongly hygroscopic, higher humidity should negatively impact the QE of the PC [19]. The reason we use CsI as the PC material is, that it can be coated onto THGEMs in a facility at the TUM and that it isn't as sensitive to external influences as other PC materials. Another factor is that because of the involvement of the TUM in the HADES experiment, there is a lot of expertise on coating CsI at the TUM [14].

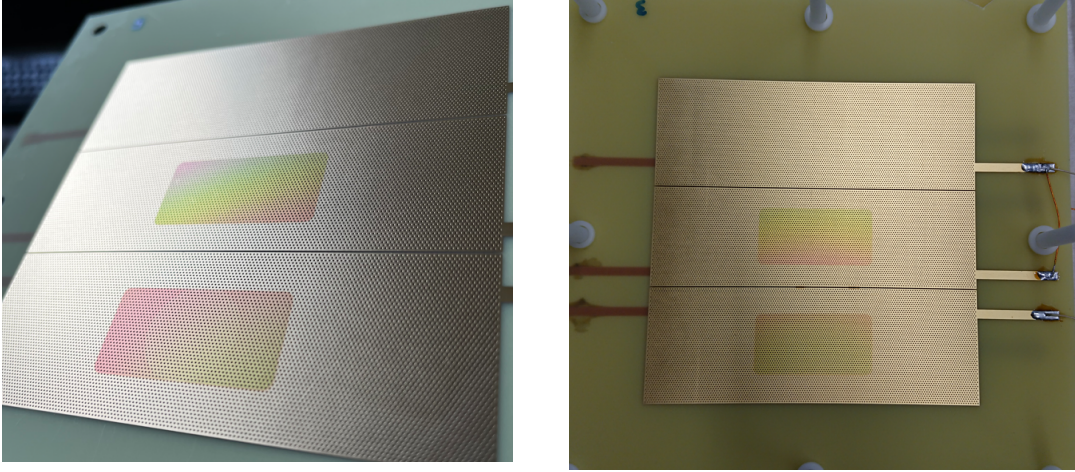


Figure 10: *Left figure:* CsI coated THGEM after completion of measurements. The thickness of this CsI PC was 192 nm, which was measured at the clean room coating facility at the TUM. One can see an indication of a circle on the bottom coated area. This was due to this area being illuminated by the lamp, as it was directly beneath the hole of the aperture. *Right figure:* CsI coated THGEM with cables attached. The THGEM, sectioned in three segments, had two parts coated with CsI.

## 2.3 Methodology

There are multiple electric fields -  $E_{suck}$ ,  $E_{stop}$  and  $E_{ind}$  - that are kept constant throughout the various measurements. The electric field between the aperture and mesh is set to  $E_{suck} = -1000 \text{ V/cm}$  to prevent any outside electrons from entering the lower stages of the setup. The electric field between the mesh and wires is set to  $E_{stop} = 170 \text{ V/cm}$ . The idea behind this is, that if electrons, which are emitted by the PC and not drawn into the hole by the dipole field of the THGEM, are between the wires and mesh, they get accelerated back towards the wires, where we can detect them as the current  $I_{wires}$ .

$E_{ind}$ , the field between THGEM bot and anode, is kept at  $0 \text{ V/cm}$ . This is done, because the setup used only utilizes one THGEM, and therefore when performing gain measurements, the electrons leaving the hole can be recorded at THGEM bot. This is explained in detail in section 2.3.1.

To ensure consistent output during a measurement series, the UV-lamp requires a certain warm-up time. As the lamp has been in use for over 20 years and is well beyond its product lifetime, the warm-up time has to be determined experimentally. To do this, the lamp was turned on and the current at all electrodes was constantly measured. After a certain time the currents were stable at the electrodes. When the currents don't change in value then the output of the lamp is consistent. We determined that before taking measurement, the lamp has to warm up for at least two hours to deliver constant output. Fluctuations in day to day operation are observed and are taken into account. These fluctuations are observed when comparing the current  $I_{suck}$  from different measurements at a setting of  $U_{aperture} = -350$  V. The negative aperture voltage leads to an electric field between the aperture and the detector vessel, which will accelerate electron away from the aperture. Because of the workfunction of Alumimium (see table 2) photoelectrons are emitted from the aperture during the measurements. Due to the electric field these electrons are accelerated away from the aperture and therefore the positive current  $I_{suck}$  corresponds to the number of emitted photoelectrons. This means that  $I_{suck}$  only depends on the output of the lamp. Ultimately we can compare the output of the lamp during various measurements, as long as they were done with the same filter and in the same medium (gas or vacuum). This allows us to compensate for the unstable output of the lamp from day to day operation by normalizing the currents to the recorded value of  $I_{suck}$  at  $U_{aperture} = -350$  V for each measurement series.

The calibration process before each measurement consists of waiting for the lamp to warm up, then closing the vacuum valve to stop the UV-light from entering the detector vessel and applying the required voltages to each electrode. It takes a couple of minutes for all current values to have settled. After this, the software calculates the mean value of the offset for each current. This completes the calibration process after which the vacuum valve is reopened and the measurements begin, with the advantage, that the recorded values are corrected for the offset.

### 2.3.1 Gain

Gain is defined as the ratio of the number of electrons entering the hole and the number of electrons leaving the hole. This ratio is greater than one when multiplication in the hole starts occurring.

$I_{prim}$ , which corresponds to the current of the initial electrons entering the hole, cannot be measured directly with the setup we use. This is due to the fact, that the positive current at THGEM top during gain measurements, not only corresponds to the emitted photoelectrons, but also to gas ions, which have a positive charge and therefore get forced on to THGEM top by the electric field of the THGEM. There are ways of determining  $I_{prim}$  indirectly, which are described in section 3.2.1.

The basic settings for the gain measurements are, that we increase  $\Delta U_{THGEM}$ , while keeping  $E_{ind}$  at zero volt per cm, which means that all of the multiplied electrons will be deposited at THGEM bottom, as they follow the dipole field lines of the THGEM. Therefore, the absolute value of  $I_{GB}$  represents the amount of mul-

### 2.3 Methodology

tiplied electrons leaving the hole. If  $E_{ind}$  were be positive, some electrons would be accelerated toward the anode and then the value for the amount of multiplied electrons would be the sum of  $I_{GB}$  and  $I_{anode}$ . The drift field is  $E_{drift} = 0 \text{ V/cm}$ . The reason for this is discussed in section 3.2.

Ultimately the gain can be calculated by using the following equation:

$$Gain = \frac{|I_{GB}|}{I_{prim}}. \quad (2)$$

#### 2.3.2 Quantum efficiency

The quantum efficiency (QE) of a PC material is the probability, that if a photon hits the PC, a photoelectron is emitted. This depends on the work function of the PC material and the wavelength of the incoming photon. QE values are usually determined with measurements done in vacuum conditions.

The wavelength of the incoming photon is quite difficult to define in our experiment, because the Deuterium lamp has a broad wavelength spectrum, which can be seen in figure 11. This is the reason we use filters for the measurements. The filter being used for QE measurements is the 171 nm-filter and its transmission can be viewed in figure 30. Applying this filter leads to a very narrow wavelength spectrum at a wavelength of around 161 nm, as can be seen in the right plot of figure 11.

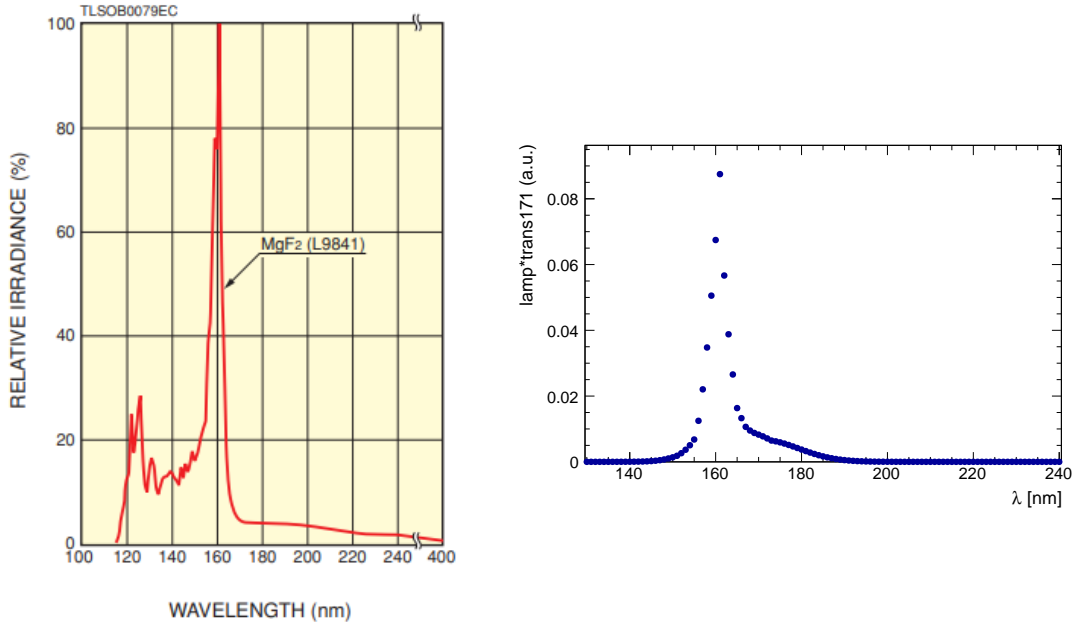


Figure 11: *Left picture:* The wavelength spectrum of the used Deuterium lamp. The relative intensity is highest for wavelengths around  $\lambda = 161 \text{ nm}$  due to the built-in  $\text{MgF}_2$  window [20]. The energy of the emitted photons range from  $E_{photon} = 5.64 - 10.78 \text{ eV}$ . *Right picture:* The output of the lamp is folded with the transmission of the 171nm-filter.

### 2.3 Methodology

To calculate QE, we need to compute the ratio between the number of photons illuminating the PC and the number of photo electrons emitted by the PC.

The amount of photons which hit the PC is extracted by doing reference measurements with a diode, which will now be discussed. The dimensions of the active area of the diode (Thorlab FGAP71 diode) are 2.5 mm x 2.5 mm. For the diode measurement the THGEM and anode are extracted from the setup and replaced by a PVC plate with holes to position the diode. The distance between the diode and the light source is the same as the distance between the light source and THGEM. Every other electrode is left in its original place. Therefore we can assume that the same amount of photons per area is hitting the PC and the diode, because in both setups the mesh and wires are in the same position and have a transparency of 51%.

To begin the measurement process, the vacuum pump is started and left to pump for around seven hours to reach a pressure inside the detector vessel of around  $p = 5 \cdot 10^{-6}$  mbar. Then the 171nm-filter is put in place with the use of the filter wheel and after the completion of the calibration process, the current at each remaining electrode is measured with the pA-meter, while the Keithley electrometer is used to measure the current of the diode. It is important to note, that the electric fields  $E_{stop} = 167$  V/cm and  $E_{suck} = -1000$  V/cm were kept constant. To achieve this value for  $E_{suck}$  the voltage at the aperture was set to  $U_{aperture} = -350$  V. As mentioned above at this specific setting for the aperture voltage we can compare this measurement to other measurements done with the same filter in vacuum.

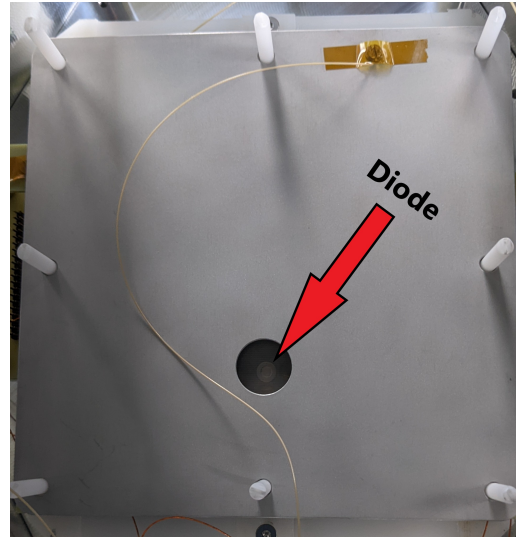
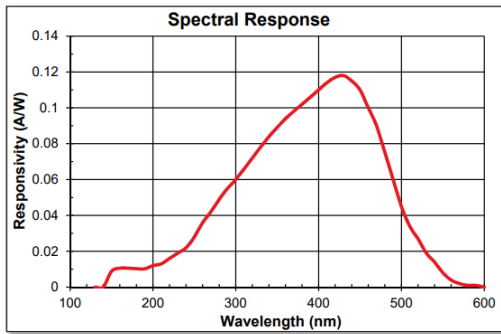


Figure 12: *Left picture:* The spectral response of the diode, used for reference measurements to determine the QE of the CsI coating.[21]. *Right picture:* This picture shows an example of the Diode measurement. The diode is placed in the middle of the hole in this picture.

This process is repeated for different positions of the diode in the PVC plate. This is important, because the intensity of the lamp light is not uniform across the illuminated area. Therefore the current of the diode  $I_{diode}$  is different for each

position. Because the reference diode measurement are only completed for a limited number of diode positions, the average of the recorded currents has to be drawn. This average has to then be multiplied by the QE value of the diode at a wavelength of  $\lambda = 161$  nm (see left plot in figure 12) and has to be multiplied by a factor that takes the active area of the diode versus the active area of the PC into account. The details of this calculation will be discussed below. Figure 12 shows the changed setup used during the diode measurement.

After the reference measurement with the diode, determining the amount of emitted electrons in vacuum is the next step to calculate QE. For this we set  $\Delta U_{THGEM} = 0$  V and increase the electric field  $E_{drift}$  to high negative values, which accelerates the electrons from the PC toward the wires. We call this measurement e-to-wires measurement. It will be referred to as such throughout this thesis. A sketch of the e-to-wires measurement can be seen in figure 13.

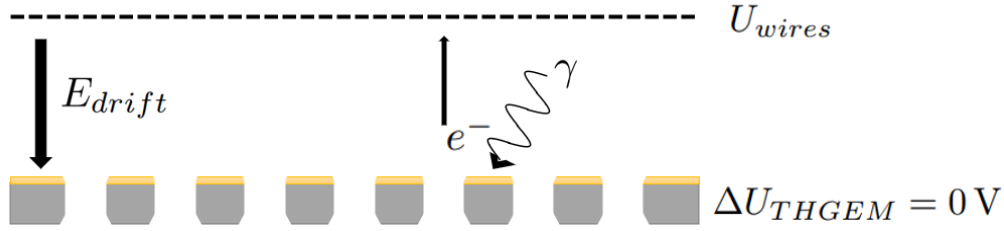


Figure 13: This picture highlights the movement of the emitted photoelectrons during the e-to-wires measurement. The electric field  $E_{drift}$  is negative so that electrons emitted from the PC get accelerated to the wires.

At high negative electric drift field values in vacuum we expect the current  $I_{GT}$  to be constant (explanation in section 3.1). Therefore the average value of  $I_{GT}$  during the e-to-wires measurement, where the current is constant at high drift field, is used for further QE calculations.

After obtaining the required values the QE is calculated with the following formulas. First the solid angle  $\Omega$  for the PC and diode are calculated with formula (3).

$$\Omega = \frac{A}{r^2} \quad (3)$$

The variable  $A$  corresponds to the active area, while  $r$  stands for the distance from the lamp, which is  $r = (296 \pm 4)$  mm. The next step is to determine the photon rate  $R_{ph}$ . This is done with the help of equation (4).

$$R_{ph} = \frac{I_{diode}}{e \cdot QE} \quad (4)$$

The photon rate is the division of the average diode current  $I_{diode}$  by the electron charge  $e$  and the QE of the diode at a wavelength of around  $\lambda = 161$  nm, which is  $8 \pm 1\%$ .

With this we can calculate the photon rate of the PC as (5)

$$R_{phPC} = R_{ph} \cdot \frac{\Omega_{PC}}{\Omega_{diode}}. \quad (5)$$

## 2.3 Methodology

After this we have to calculate the number of electrons released from the PC per second during the e-to-wires measurement with  $N_e = \frac{IGT}{e}$ . The last step is to calculate the QE of the CsI PC with equation (6).

$$QE_{CsI} = \frac{N_e}{R_{phPC}} \quad (6)$$

Every uncertainty provided in this bachelor's thesis is calculated with the use of the equations given in [22].

### 2.3.3 Aging

Aging studies are performed to investigate the decline of the quality of the PC in terms of QE. One aspect of this research is to determine the impact of long exposure times to gas on the QE of the PC. To investigate this, e-to-wires measurement in gas, in our case Ar-CH<sub>4</sub> (90-10), at identical settings are performed twice a day for seven days.

Another aspect is to understand which impact constant bombardment of gas ions during gain measurements has on the QE of the CsI. For this purpose e-to-wires measurements in vacuum are performed right after gain measurements. During gain measurements, gas ions produced in the hole will travel to and be deposited on to the PC because of the electric field of the THGEM. The e-to-wires measurement after each gain measurement allows us to determine, which impact the ion bombardment has on the QE of the PC. To quantify this impact, we calculate the charge per area. The charge, which is equivalent to the ions hitting the PC, is computed by integrating the current  $I_{GB}$  over the measurement period. This is done after each gain measurement. Each charge value is divided by the illuminated area of the PC to obtain a value for the charge per area, which is deposited onto the PC during gain measurements.

### 3 Results and discussion

#### 3.1 E-to-wires measurement

##### 3.1.1 In vacuum

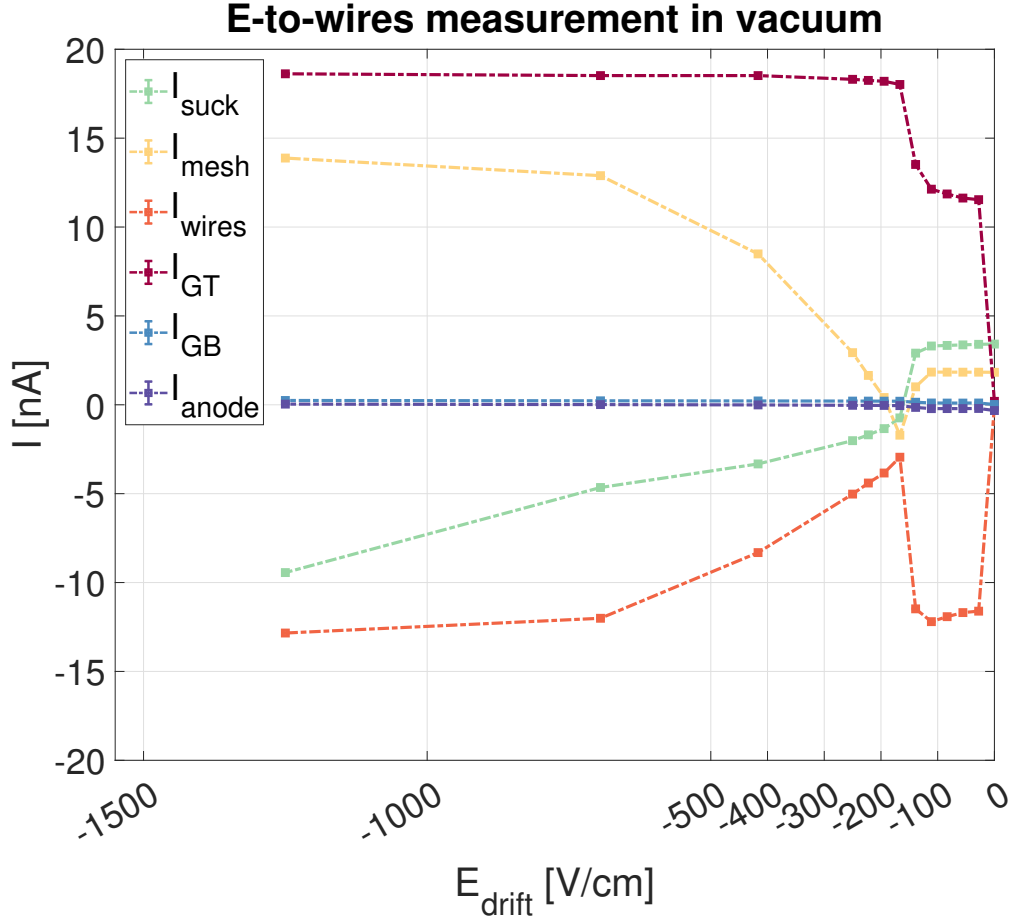


Figure 14: Currents at each electrode plotted against the drift field  $E_{drift}$ . The filter  $\text{CaF}_2$  and the CsI 195 nm thick coated THGEM were used.

Figure 14 displays the currents measured at each electrode as a function of the increasing electric field  $E_{drift}$  in vacuum. This measurement was performed with the  $\text{CaF}_2$  filter and the CsI 195 nm thick coated THGEM.

The basic idea behind the e-to-wires measurement is to determine the number of photoelectrons leaving the PC. If there is a negative electric field between THGEM top and wires, emitted photoelectrons will travel away from the PC and towards the wires. This results in a positive current on the topside of the THGEM  $I_{GT}$ , which corresponds to the number of emitted photoelectrons. Because these electrons travel towards the wires and should be collected there, the negative current  $I_{wires}$  should also correspond to the number of emitted photoelectrons. In vacuum, this isn't the case, because the velocity of the electrons can get so high, that electrons can move past electrodes without being collected. This is quite apparent

### 3.1 E-to-wires measurement

when comparing  $I_{GT}$  and  $I_{wires}$  in figure 14.

In the low drift field ( $\approx -150$  V/cm) region the absolute values of these two currents are the same, which is expected, as each electron leaving the top side of the THGEM drifts toward the wires and is detected there as a negative current. But at high drift fields, the electrons are accelerated to such high velocities that they aren't collected at the wires. For example for the setting of  $E_{drift} = -1250$  V/cm, the current at THGEM top is  $I_{GT} = (18.62 \pm 0.02)$  nA while the current at wires is  $I_{wires} = (-12.84 \pm 0.01)$  nA.

It is also interesting to note the behavior of  $I_{GT}$ . There are two regions of interest: The first region is in the low drift field region, where  $I_{GT}$  is quite steadily increasing. In the second region at higher drift fields,  $I_{GT}$  all of a sudden increases in value and from there on out is constant. The sudden jump in value for  $I_{GT}$  is still not understood. Other researchers report similar behavior but do not explain why this occurs [23].

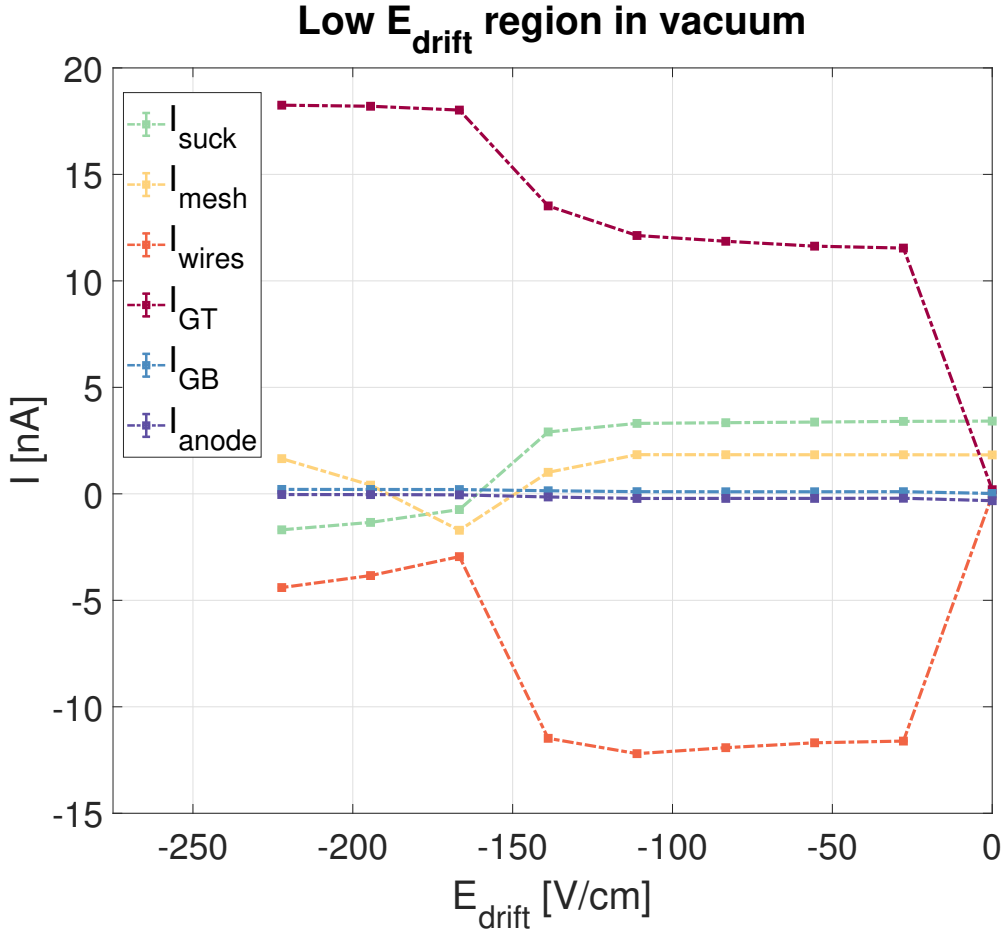


Figure 15: This plot shows the low drift field region recorded during the e-to-wires measurement in vacuum. The filter  $\text{CaF}_2$  and the CsI 195 nm thick coated THGEM were used.

It is interesting to note, that as  $I_{GT}$  suddenly increases in value,  $I_{wires}$  decreases.

### 3.1 E-to-wires measurement

When the electrons are accelerated to such high velocities that they pass through the wires and travel through  $E_{stop}$  without getting stopped, then this explains the decrease in the current  $I_{wires}$ . When moving through  $E_{drift}$  the electrons get accelerated. The energy of the electrons can be calculated with  $E_{kinetic} = \Delta U_{GT-wires} \cdot e$ , where  $\Delta U_{GT-wires}$  stands for the potential difference between THGEM top and the wires.

The electric field  $E_{stop}$  with the energy  $E_{kinetic} = \Delta U_{wires-mesh} \cdot e$ , where  $\Delta U_{wires-mesh}$  stands for the potential difference between the wires and the mesh, slows the electrons down. If  $\Delta U_{GT-wires} > \Delta U_{wires-mesh}$ , then the electrons have enough energy to pass through the electric field  $E_{stop}$ . This happens at  $\Delta U_{GT-wires} > 50$  V, which corresponds perfectly to the  $\Delta U_{GT-wires}$  setting at an electric drift field of around 150 V/cm. Therefore the electrons move through  $E_{stop}$  without being stopped and aren't detected at the wires anymore.

But this doesn't explain the increase in  $I_{GT}$ . There is a theorem, called the Ramo-Shockley theorem, that explains the correlation between a current  $i$  measured at an electrode and the velocity of a charged particle in its vicinity in an electric field. The equation describing this is  $i = e \cdot v \cdot E$  [24]. The reason this can't explain the increase of  $I_{GT}$  is, that this effect should result in a constant increase of  $I_{GT}$  at increasing drift fields. This is not the case, as the current  $I_{GT}$  is constant at high drift fields. Lastly, there is one other solution that could potentially explain the increase in  $I_{GT}$ . At a drift field of  $E_{drift} \approx -150$  V/cm, the electric field might penetrate further into the PC and therefore promote the emission of more photoelectrons. This enhancement of photoelectron emission is usually observed at very high electric fields ( $> 500$  kV/cm), where secondary photoelectrons are emitted [25]. It could potentially be possible that a similar effect at a low electric field  $E_{drift}$ , while less pronounced, could result in a decrease in the work function of the CsI PC and therefore leading to more photoelectrons being emitted.

The current  $I_{anode}$  and  $I_{GB}$  remain zero because there is no applied induction field  $E_{ind}$  and no potential difference  $\Delta U_{THGEM}$ . This is also the case in the e-to-wires measurement in gas.

The behavior of the currents  $I_{stop}$ ,  $I_{suck}$  and the apparent change in currents at negative drift fields higher than  $-150$  V/cm is still not completely understood and has to be researched in more detail.

The current at the aperture  $I_{suck}$  increases with the electric drift field  $E_{drift}$ . A possible explanation could be that as the electric drift  $E_{drift}$  increases, photoelectrons from the PC either hit the aperture or go through the hole of the aperture. As mentioned above at a drift field of  $E_{drift} \approx -150$  V/cm the photoelectrons have enough energy to move through  $E_{stop}$ . Because there is a voltage at the aperture  $U_{aperture}$ , this not only creates the electric field  $E_{suck}$ , but also an electric field between the aperture and detector vessel. At  $E_{drift} = 0$  V/cm the voltage at the aperture is  $U_{aperture} = -350$  V. But as the drift field increases, the voltage at the aperture is reduced, because every other electric field in the setup has to stay the same during the e-to-wires measurement. For the maximal drift field for example this results in  $U_{aperture} = 0$  V. The electrons, which get accelerated through the hole of the aperture, end up in the detector volume above the aperture. At a low voltage at the aperture, electrons are more likely to stick to the aperture. This in

essence would explain the high negative current observed at the aperture when having a high drift field and therefore low voltage at the aperture.

This theory doesn't apply to the region of the drift field between  $E_{drift} = 0$  to  $-150$  V/cm, because  $I_{suck}$  is positive in this case. This is due to the fact, that photoelectrons are emitted and accelerated away from the aperture. Therefore, the positive current  $I_{suck}$  at a setting of  $U_{aperture} = -350$  V allows us to monitor the output of the lamp. Ultimately this means, that at high aperture voltage settings the current  $I_{suck}$  only depends on photoelectrons emitted by the aperture. This is contrary to the case at low aperture voltage, where we assume that photoelectrons from the PC influence  $I_{suck}$ .

Next, the behavior of  $I_{stop}$  is discussed. The growing positive current at  $E_{drift}$  larger then  $-150$  V/cm indicates that electrons are leaving the electrode. The work function of Tungsten would allow for the emission of photoelectrons. But why a change in voltage at the electrode should change this emission rate, especially as the electric fields around the electrode don't change, is not clear. One thing that is also interesting is that the values of the current at wires and mesh seem to offset each other in the high drift field region. This would mean, that photoelectrons emitted by the mesh are accelerated towards the wires due to  $E_{stop}$  and collected there. It has to be noted, that this still does not explain why these currents are growing. Similar to the case of  $I_{suck}$  at the region of the drift field between  $E_{drift} = 0$  and  $-150$  V/cm, the current is positive and constant because photoelectrons are emitted from the mesh in a constant rate. These electrons end up drifting towards the detector housing, as there is no corresponding negative current being measured.

Finally, the biggest mystery is the change in behaviour which can be seen for every current (except  $I_{anode}$  and  $I_{GB}$ ) when going from a drift field region of  $E_{drift} = 0$  and  $-150$  V/cm to a region greater then  $E_{drift} = -150$  V/cm. This change is not only seen when measuring with the  $\text{CaF}_2$  filter but also with  $\text{SiO}_2$  and  $171\text{nm}$ -filter and this change always happens at the same drift field configuration. As mentioned above, this might be due to to the velocity the photoelectrons from the PC reach at that specific drift field setting, which allows them to move past the other electrodes. The behavior of the measured currents in the low drift field region can be seen in figure 15.

Ultimately the interesting part of this measurement, apart from understanding the electron movement inside the detector, is to get a value for the maximum number of photoelectrons leaving the CsI PC. This is why for QE measurements the only current of interest is  $I_{CT}$  at high drift field settings, where it is constant.

#### 3.1.2 In gas

Figure 16 shows the e-to-wires measurement in  $\text{Ar}-\text{CH}_4$  (90-10). This measurement was done a day apart from the one in vacuum with the same filter and coated THGEM. In gas the electrons reach a finite drift velocity, which depends on the electric drift field  $|\vec{E}|$  and the mean interaction time  $\tau$  [26].

As can be seen in the figure 16, the currents  $I_{wires}$  and  $I_{GT}$  offset each other for

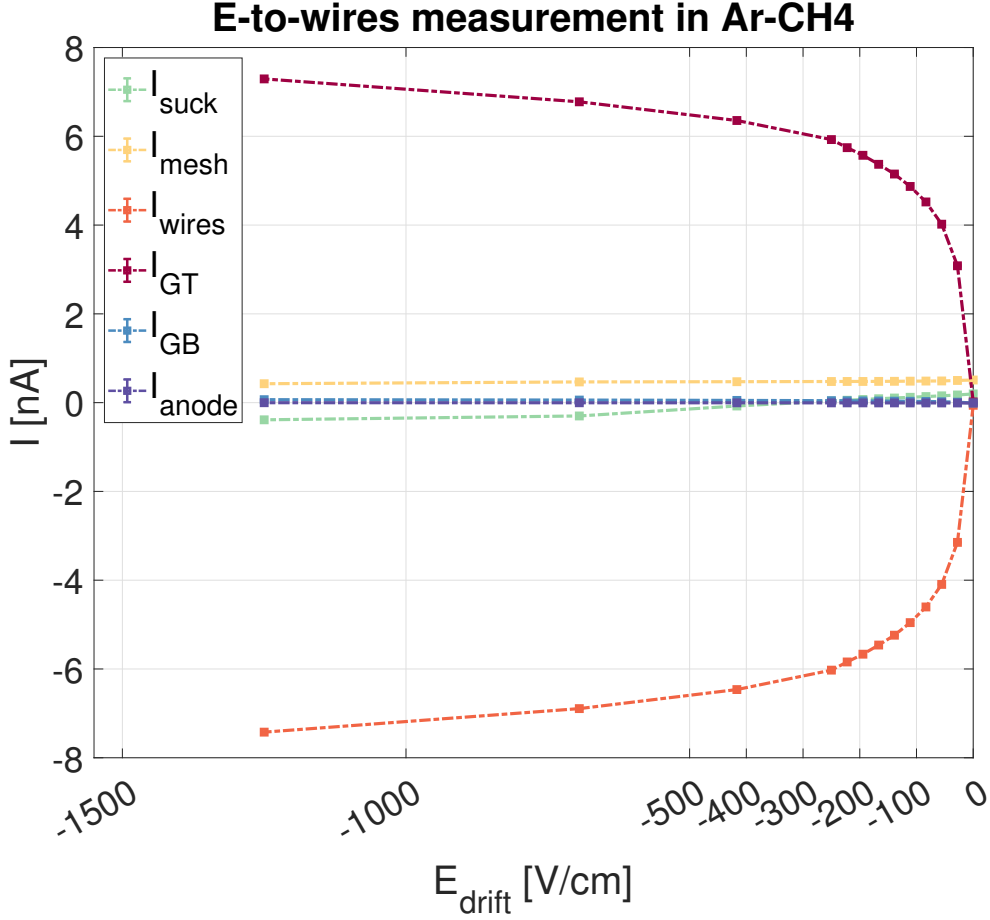


Figure 16: Currents measured at each electrode plotted against the drift field  $E_{drift}$ . The filter  $\text{CaF}_2$  and the CsI 195 nm thick coated THGEM were used.

the whole drift field range. This means that all electrons, which are emitted from the PC, do not have enough energy to pass  $E_{stop}$  and are therefore collected at the wires.

The value of  $I_{GT}$  increases with the electric field  $E_{drift}$ . This we expect, because the stronger the electric field, the less electron backscattering - which describes the process, in which an emitted photoelectron elastically scatters at a gas atom and gets reabsorbed into the PC - plays a role. At higher electric fields the electrons predominately collide inelastically with gas atoms and not elastically anymore [27]. This not only depends on the electric field strength at the PC but also on the gas used [28]. The effect of electron backscattering plays a bigger role in pure noble gases than for example in the gas mixture used in this experiment, Ar-CH<sub>4</sub> (90-10), because pure noble gases have an enhanced cross-section for elastic scattering [11].

The maximum current at the top side of the THGEM in gas is lower than that in vacuum, as in vacuum there is no backscattering of electrons.

Similar to the case in vacuum no current at the anode and THGEM bot is measured. The current on the aperture  $I_{suck}$  decreases with an increase in drift field.

### 3.2 Gain measurement

At higher drift field settings, the voltage on the aperture decreases, and therefore the electric field between detector vessel and aperture decreases. This means more photoelectrons from the aperture are reabsorbed due to electron backscattering. The current  $I_{stop}$  is positive and constant, which means photoelectrons are emitted from the mesh at a constant rate.

To keep  $\Delta U_{THGEM} = 0$  V, we set  $U_{GT} = U_{GB} = -500$  V. This poses a problem, as fluctuations in the outputs of the high voltage power supply lead to uncertainties for  $I_{GT}$  and  $I_{GB}$ , which are in the order of  $10^{-2}$  nA. For e-to-wires measurement with CsI coated THGEMs, this has very limited impact, as the measured currents are two orders of magnitude higher. But when performing measurements with materials that have very low QE in the UV region, for example, DLC GEMs or uncoated Au THGEMs, the uncertainties are in the same order of magnitude as the measured currents. This problem can be corrected by splitting one output of the voltage supply into two cables, which then supply the same voltage to THGEM top and bottom. To validate this approach, we took an e-to-wires measurement with the improved setup in gas with  $U_{GB} = U_{GT} = -500$  V and compared it to an e-to-wires measurement (same gas, filter, and THGEM), where we grounded THGEM top and bottom while adjusting the voltages at the other electrodes to keep all electric fields at the same strength. This comparison is shown in figure 34 in the appendix.

### 3.2 Gain measurement

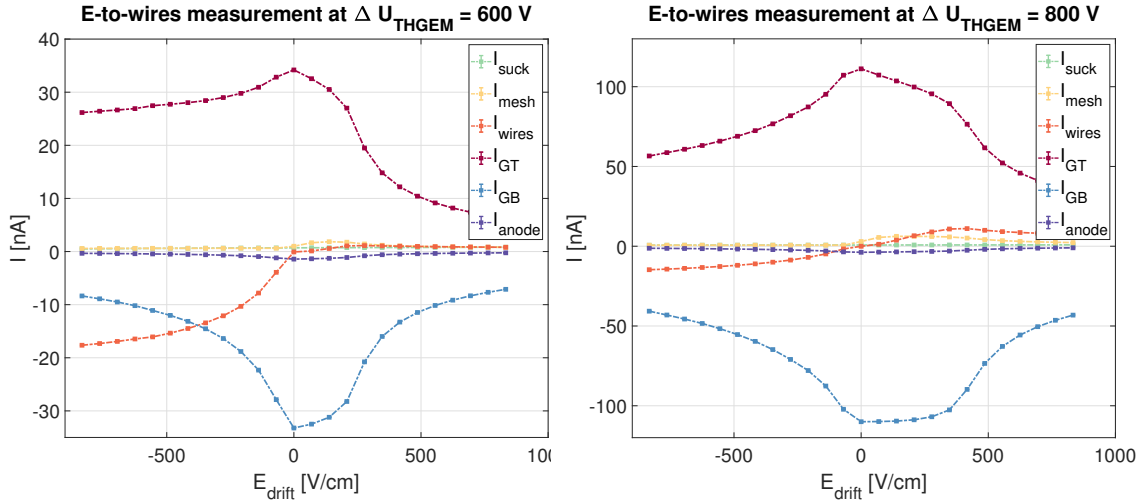


Figure 17: *Left plot:* An  $E_{drift}$  scan at  $\Delta U_{THGEM} = 600$  V. *Right plot:* An  $E_{drift}$  scan at  $\Delta U_{THGEM} = 800$  V. These measurements were performed with the CsI 195 nm thick coated THGEM and the  $\text{CaF}_2$  filter in  $\text{Ar}-\text{CH}_4$  (90-10).

Gain measurements with  $\text{Ar}-\text{CH}_4$  (90-10) are performed to understand what gain can be reached with our single THGEM setup. This is vital for the application of THGEMs as photodetectors because, without a sufficient multiplication of photoelectrons in the holes of the THGEM, photons cannot be detected.

## 3.2 Gain measurement

To perform gain measurements,  $\Delta U_{THGEM}$  is increased, which strengthens the dipole field of the THGEM and accelerates electrons through the hole. In the holes, electrons ionize gas atoms, if they have sufficient energy to do so, and therefore create an electron avalanche. While increasing  $\Delta U_{THGEM}$ , the drift field is kept at  $E_{drift} = 0 \text{ V/cm}$ . The reason for this can be seen in figure 17. These measurements are  $E_{drift}$  scans, which are performed at a fixed  $\Delta U_{THGEM}$  in gas. The potential difference  $\Delta U_{THGEM}$  of both measurements is at a level, where the multiplication of electrons in the holes happens. The reason for performing this measurement is to determine at which  $E_{drift}$  setting the most electrons enter the hole. One can clearly see, that the current  $I_{GT}$  for both plots is at a maximum at  $E_{drift} = 0 \text{ V/cm}$ .

A positive electric drift field would force some emitted photoelectrons to reenter the PC. This must be avoided, as this would result in the loss of a signal. A negative drift field, on the other hand, would force some electrons to accelerate toward the wires and not toward the holes. It should be mentioned that even at potential differences  $\Delta U_{THGEM}$ , which were higher than the ones we measured and at which THGEMs are usually operated,  $E_{drift} = 0 \text{ V/cm}$  is the best operational setting for these detectors [29].

The amount of initial electrons entering the hole is  $I_{prim}$ . This current cannot be measured directly with our setup, but there are other ways of determining it.

### 3.2.1 Linear fitting to plateau

One way to do this is to plot  $|I_{GB}|$  half logarithmic against  $\Delta U_{THGEM}$ . The current  $I_{GB}$  corresponds to the number of electrons leaving the hole of the THGEM during gain measurements. This current equals  $I_{prim}$ , if all initial electrons go through the hole, without initiating an electron avalanche, and end up on the bottom side of the THGEM. This happens at a potential difference  $\Delta U_{THGEM}$ , where the dipole field is so strong, that the maximum amount of electrons are emitted from the PC, but too weak to lead to electron multiplication in the hole. This region can be seen as a plateau in the left plots of figure 21 and 22. When fitting a linear function to this region, one can obtain a value for  $I_{prim}$ . The obvious drawback of this method is, that it is difficult to define this region because it is impossible to know at which exact potential difference  $\Delta U_{THGEM}$  electron multiplication starts taking place.

### 3.2.2 E-to-wires measurement

There is another method to obtain  $I_{prim}$ . The number of initial electrons in gas can be determined by looking at the e-to-wires measurement. Here the amount of emitted photoelectrons corresponds to the current  $I_{GT}$  at high negative drift fields. This value should correspond to the amount of initial electron  $I_{prim}$  in gain measurements if we assume that every emitted photoelectron gets guided into the hole by the dipole field of the THGEM. This assumption is not correct, because the efficiency of drawing the electrons is smaller than 1, as can be seen when comparing figure 18 to figure 19.

### 3.2 Gain measurement

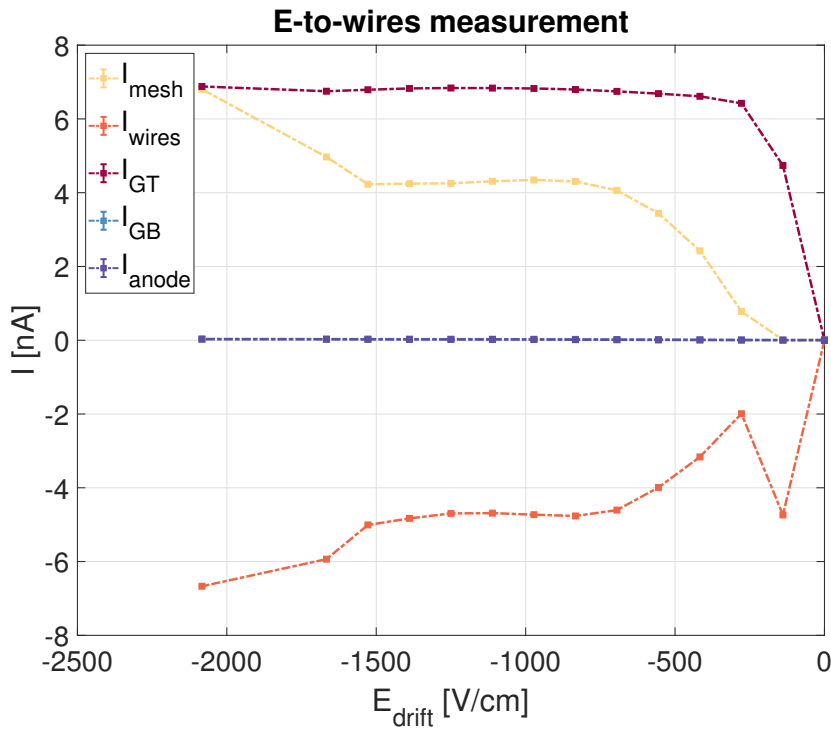


Figure 18: The measured currents plotted against the  $E_{drift}$ . The current  $I_{suck}$  is not shown, as it would distort the graph. The 171nm-filter and CsI 205 nm thick coated THGEM in vacuum was used.

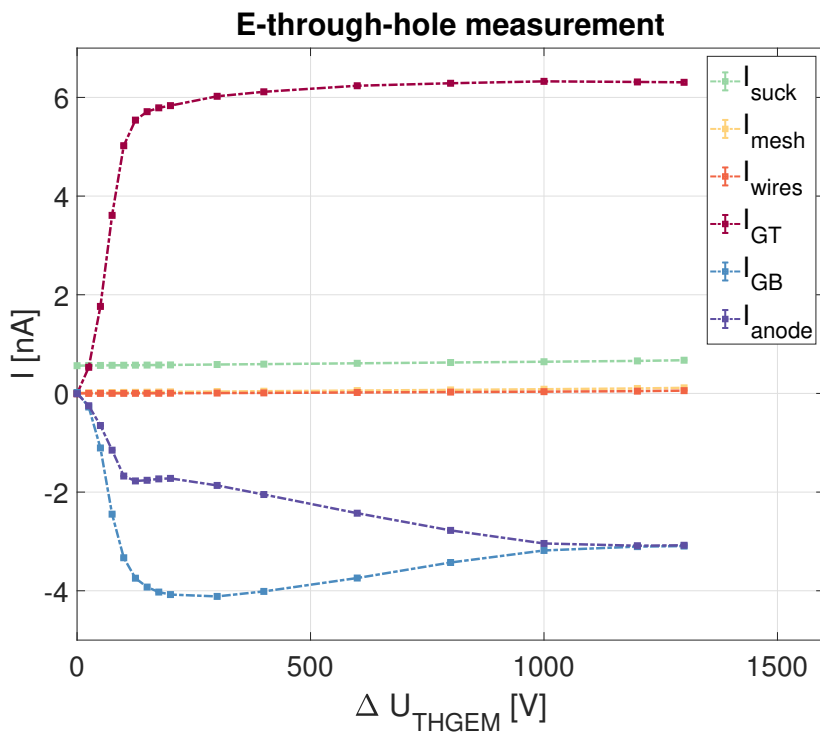


Figure 19: The measured currents plotted against the  $\Delta U_{THGEM}$  at the THGEM. The 171nm-filter and CsI 205 nm thick coated THGEM in vacuum was used.

Figure 18 shows an e-to-wires measurement in vacuum and figure 19 a measurement we call e-through-hole measurement, which is similar to a gain measurement. The only difference is that e-through-hole measurements are performed in vacuum. This means the electrons get accelerated through a hole but, because there are no gas atoms, no electron avalanche is initiated. A sketch displaying the electron movement during this type of measurement can be seen in figure 20.

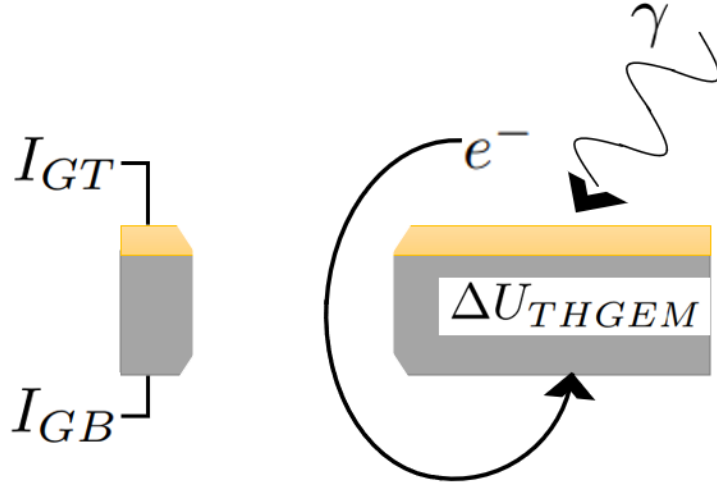


Figure 20: The electron movement during an e-through-hole measurement. There is no electron multiplication because this measurement is performed in vacuum.

The e-to-wires and e-through-hole measurement were done on the same day with the same filter and coated THGEM. Regarding figure 19, it should be mentioned that the currents  $I_{GB}$  and  $I_{anode}$  behave differently in gas. In vacuum the electrons, which get accelerated through the hole, end up either on the anode or THGEM bottom. The fraction of electrons landing on either electrode depends on the potential difference and therefore the electric field of the THGEM.

For a potential difference of around  $\Delta U_{THGEM} = 1200 \text{ V}$  the currents have the same value. This is not surprising, as in vacuum the electrons follow the electric field lines (see figure 3) and don't collide with atoms. This isn't the case when doing gain measurements. Electrons leaving the hole will collide with gas atoms in the drift volume between THGEM bot and anode and lose kinetic energy. This results in the electrons getting drawn towards THGEM bottom and creating the detectable current  $I_{GB}$ .

Going back to the e-to-wires measurement in gas, we assume that the dipole field of the THGEM at high enough values for  $\Delta U_{THGEM}$  has the same effect as a high negative drift field  $E_{drift}$ . This means, that the electric field penetrates the PC and the maximum amount of photoelectrons is emitted. We define the efficiency to collect all emitted photoelectrons as  $\epsilon_{coll}$ . This efficiency, which is the ratio of the maximum  $I_{GT}$  of the e-through-hole measurement to the maximum  $I_{GT}$  value of the e-to-wires measurement, is  $\epsilon_{coll} = 0.919 \pm 0.004$ .

Ultimately this means that the maximum current  $I_{GT}$  of e-to-wires measurement in gas is higher than the number of initial electrons during gain measure-

ments. Looking at equation (2), the calculated gain will be underestimated.

### 3.2.3 $I_{prim}$ of CsI coated and uncoated Au THGEM

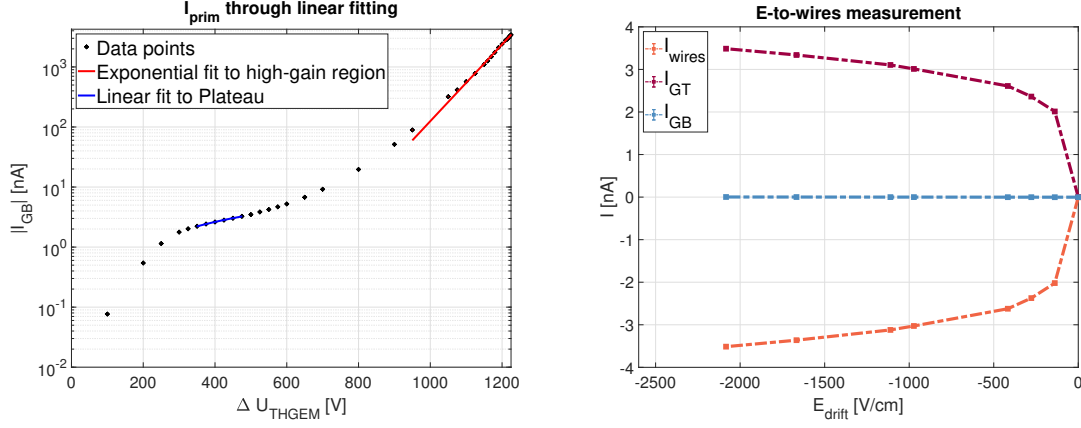


Figure 21: *Left plot:* The absolute value of  $I_{GB}$  plotted half logarithmic against the potential difference  $\Delta U_{THGEM}$ . The uncertainties are left out but can be viewed in figure 35. *Right plot:* The e-to-wires measurement in Ar-CH<sub>4</sub> (90-10). Both measurements are performed with the CsI 205 nm thick coated THGEM and the 171nm-filter.

The left plot in figure 21 shows  $|I_{GB}|$  plotted half logarithmic against  $\Delta U_{THGEM}$ . For the CsI coated THGEM one can see an indication of a plateau in the region of  $\Delta U_{THGEM} = 350$  to  $500$  V. The value for the current, which we attain from the fit, equals to  $I_{GB} = I_{prim} = (2.83 \pm 0.50)$  nA. The e-to-wires measurement in gas with the 171nm-filter and coated THGEM can be seen in the right plot of figure 21. This measurement leads to a value for  $I_{prim} = (3.49 \pm 0.25)$  nA. This value is higher than the one we attain through linear fitting of the plateau, which fits our prediction, as the number of electrons emitted in the e-to-wires measurement is greater than the number of electrons drawn into the hole while doing gain measurements.

For the uncoated THGEM (and SiO<sub>2</sub> filter) one can see an indication of a plateau in the region of  $\Delta U_{THGEM} = 250$  to  $400$  V. By fitting a linear function to this plateau, see left plot in figure 22, we attain a value of  $I_{prim} = (0.039 \pm 0.020)$  nA. The e-to-wires measurement gives a value of  $I_{prim} = (0.057 \pm 0.003)$  nA, see right plot in figure 22. While performing the e-to-wires measurement with the uncoated THGEM, we did not use the optimized setup, where we split one output of the high voltage supply to supply both THGEM bot and top. This is why the uncertainties for  $I_{GT}$  and  $I_{GB}$  are so large. This meant we couldn't use  $I_{GT}$  to obtain a reliable value for the electrons emitted from the PC. As explained in the previous section, the number of electrons leaving the PC in gas is equal to the number of electrons being collected at the wires. The current of the wires has very small uncertainty and this is why we use the maximum absolute value  $I_{wires}$  for  $I_{prim}$ .

### 3.2 Gain measurement

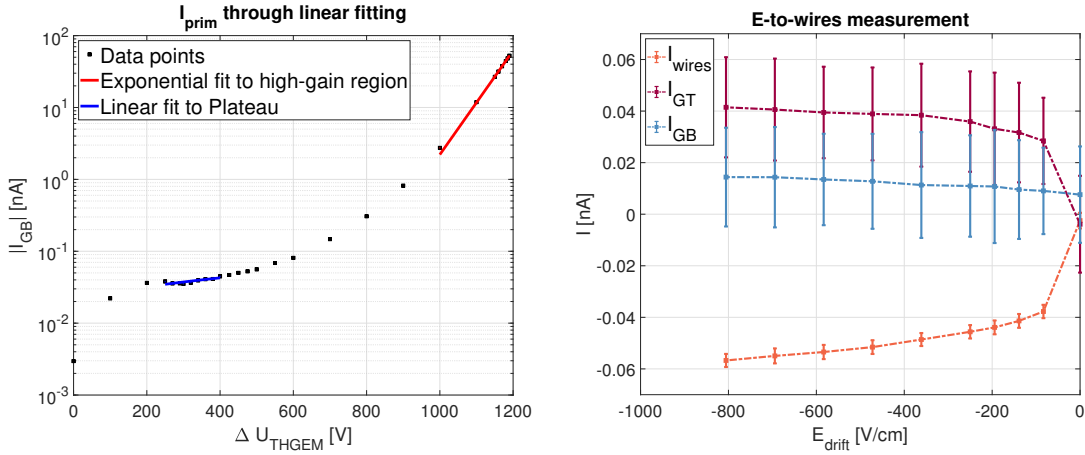


Figure 22: *Left plot:* The absolute value of  $I_{GB}$  plotted half logarithmic against the potential difference  $\Delta U_{THGEM}$ . The uncertainties are left out but can be viewed in figure 35. *Right plot:* The e-to-wires measurement in Ar-CH<sub>4</sub> (90-10). Both measurements are done with uncoated Au THGEM #5 and the SiO<sub>2</sub> filter.

#### 3.2.4 Gain of CsI coated and uncoated Au THGEM

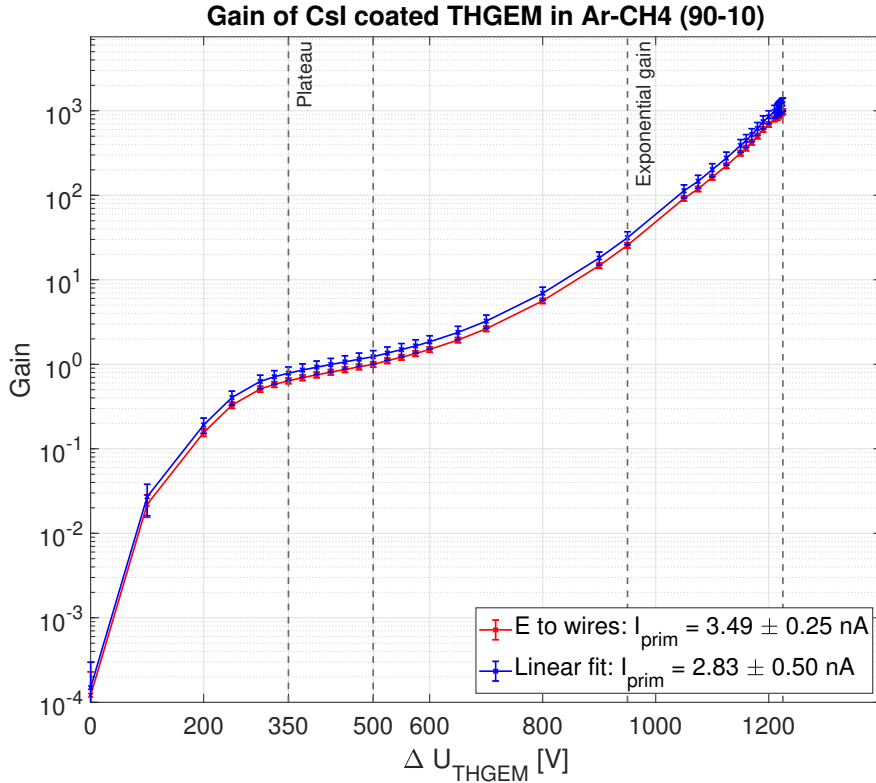


Figure 23: Gain of CsI 205 nm thick coated THGEM. The 171nm-filter was used.

Figure 23 shows the gain curves measured with CsI 205 THGEM in Ar-CH<sub>4</sub> (90-10). There are three regions of interest. At a low potential difference  $\Delta U_{THGEM}$

### 3.2 Gain measurement

(0 - 350 V), the dipole field of the THGEM is not strong enough to overcome the electron backscattering effect. Therefore the amount of electrons entering the holes is not the same amount of electrons, which will enter electron multiplication at a higher  $\Delta U_{THGEM}$  region. And because the electric dipole field of the THGEM is low in this region, the electrons don't get enough kinetic energy passing through the hole to start an electron avalanche.

The second region is the plateau region, which was discussed in the previous section. The last region is characterized by the exponential rise in the gain curve. This means that electron multiplication in the hole starts happening. The maximum gain is only limited by the onset of discharges, which starts occurring when there are enough electrons and ions in the hole to create a spark between top and bottom side of the THGEM. Discharges impact the performance of detectors in a negative way, so operating the THGEM at voltages where discharges are very rare but gain is still high is crucial [30]. At  $\Delta U_{THGEM} = 1225$  V discharges were recorded every 30 seconds, so the measurement was stopped at that point. The maximum gain that was reached with  $I_{prim}$  from linear fitting is  $Gain = 1210 \pm 213$ .  $I_{prim}$  from the e-to-wires equalled in a maximum gain of  $Gain = 984 \pm 71$ .

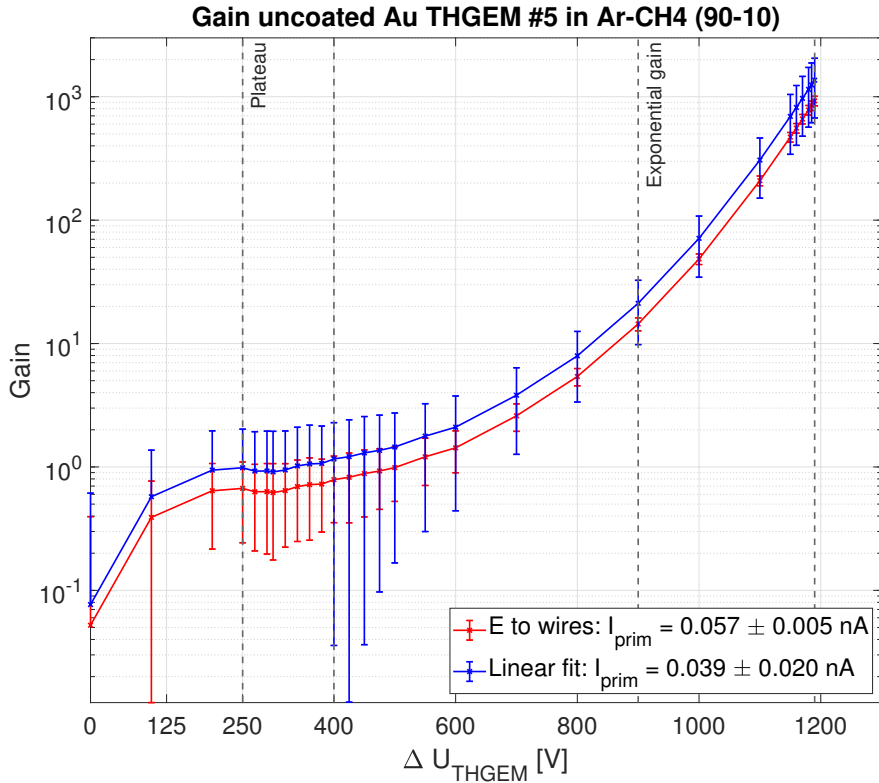


Figure 24: Gain of uncoated Au THGEM. The  $\text{SiO}_2$  filter was used.

Gain measurements with uncoated Au THGEMs were done until a potential difference of  $\Delta U_{THGEM} = 1190$  V. Discharges started occurring at this point, so no higher gain was reached. This measurement can be seen in figure 24 and as predicted, when using the  $I_{prim}$  value calculated through the e-to-wires measure-

### 3.3 Quantum efficiency of CsI PC

ment, we underestimate the gain. The exact maximum gain value with the linear fitting method is  $Gain = 1362 \pm 689$  and for the e-to-wires measurement  $Gain = 927 \pm 82$ .

Regarding the gain measurement with the coated THGEM, it has smaller uncertainties compared to gain measurements done with the uncoated THGEM. This is because the difference in order of magnitude between the measured currents and their uncertainties was higher in the case of the coated THGEM, especially in the plateau region. Both measurements were performed until a setting of  $\Delta U_{THGEM}$  was reached, where discharges occurred every thirty seconds. In the case of the coated THGEM the Keithley electrometer was used, as currents above the limit of the pA-meter were measured.

The only difference with this setup is, that the bottom side of the THGEM had to be grounded (when using the pA-meter it is set to  $U_{GB} = U_{GT} = -500$  V). As mentioned earlier, this doesn't impact the results we obtain.

### 3.3 Quantum efficiency of CsI PC

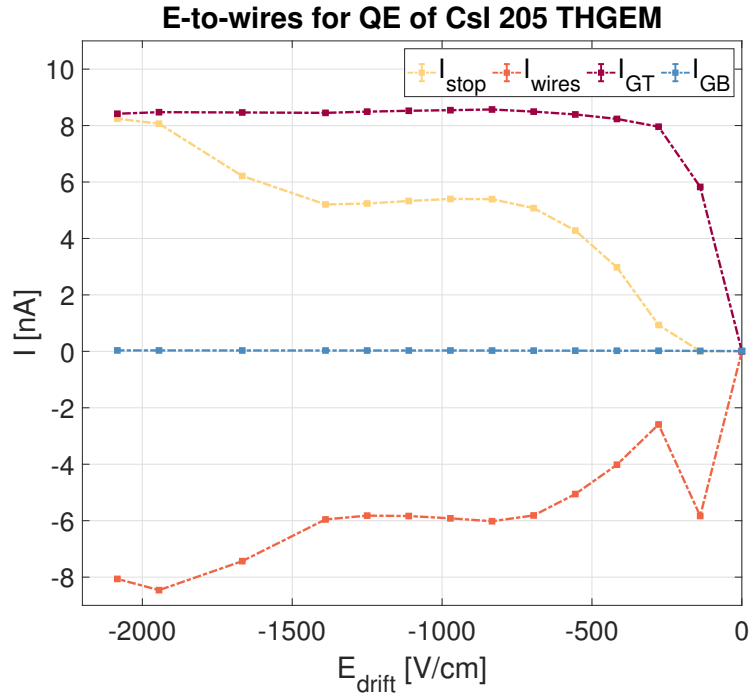


Figure 25: This is the e-to-wires measurement used to determine the number of photoelectrons leaving the CsI PC. This measurement was done in vacuum and with the 171nm-filter.

As mentioned in the methodology section, to calculate the QE of the CsI PC, two measurements have to be taken. First of all, we need the diode reference measurement to detect the number of photons hitting the active area and second of all, we need the e-to-wires measurement in vacuum to determine the number of photoelectrons being emitted by the PC.

### 3.3 Quantum efficiency of CsI PC

The latter measurement is depicted in figure 25. This measurement was performed with the  $171\text{nm}$ -filter after a series of e-to-wires measurements in gas, see section 3.4.1, which did not negatively impact the quality of the PC.

For the QE calculations, we use the average of  $I_{GT}$  in a region where it is constant. Looking at figure 25, this region is around  $E_{drift} = -700$  to  $-1300$  V/cm. The weighted average leads to a value of  $I_{GT} = (8.49 \pm 0.01)$  nA.

#### 3.3.1 Diode reference measurement

The result of the diode reference measurement can be seen in figure 26. It has to be mentioned that the values in the figure are normalized values. The reason for this is, that the output of the lamp was not constant over the measurement period. In reality, the output of the lamp decreased after each measurement, for reasons unknown to us. The original measured current with the diode, the normalized current of the diode, and the current at the aperture can be viewed in figure 32 in the appendix.

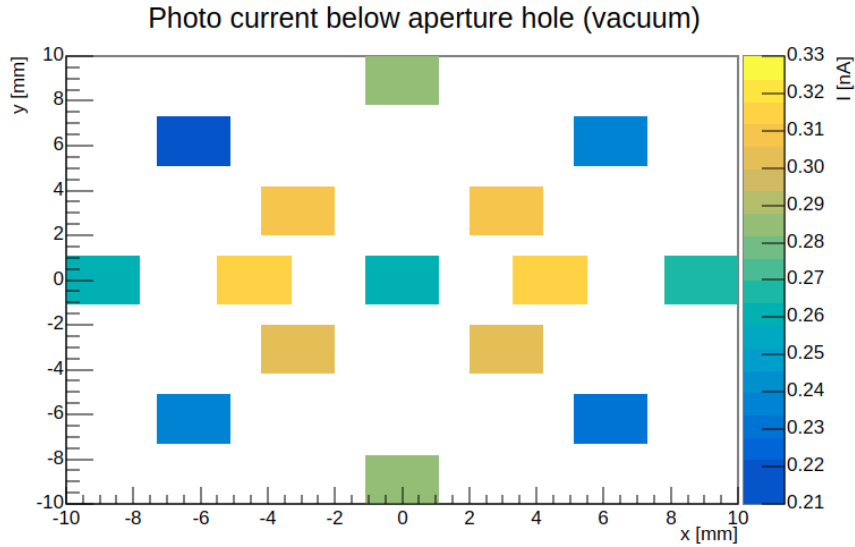


Figure 26: This plot shows the currents measured at each diode position. The used filter throughout the QE measurement process is the  $171\text{nm}$ -filter.

After normalization, the average value is calculated:

$$I_{diode} = (0.260 \pm 0.016) \text{ nA}$$

#### 3.3.2 QE calculation

The QE of the CsI 205 PC is calculated with the equations given in section 2.3.2. The active area for the PC is the area beneath the hole of the aperture and with a hole diameter of  $d = 20$  mm, we get a value of  $A = 314.2 \text{ mm}^2$ . This value has to be multiplied by the surface to hole ratio of the THGEM. Due to the unstable

### 3.3 Quantum efficiency of CsI PC

output of the lamp, the average value of  $I_{GT}$  of the CsI PC has to be normalized to the average current measured with the diode.

This is done by using the formula (7):

$$I_{GT-norm} = I_{GT} \cdot \frac{I_{suck-diode}}{I_{suck-ETW}} \quad (7)$$

In the formula above,  $I_{GT-suck}$  corresponds to the current measured at the aperture when we did our first diode measurement. As mentioned in section 2.3.2, the settings for the voltage at the aperture were identical to those later used in the e-to-wires measurement.  $I_{suck-ETW}$  on the other hand refers to the current at the aperture, which corresponds to the output of the lamp during the e-to-wires measurement in figure 25. After using the above mentioned formula we attain a value of  $I_{GT-norm} = (9.85 \pm 0.11)$  nA.

In the last step we use the equations given in section 2.3.2 to calculate the QE of the 205 nm thick CsI reflective cathode for a wavelength  $\lambda = 161$  nm:

$$QE = 7.74 \pm 0.98\%$$

It should be mentioned, that the uncertainty given does not include the systematic errors.

#### 3.3.3 Comparison to DLC GEM

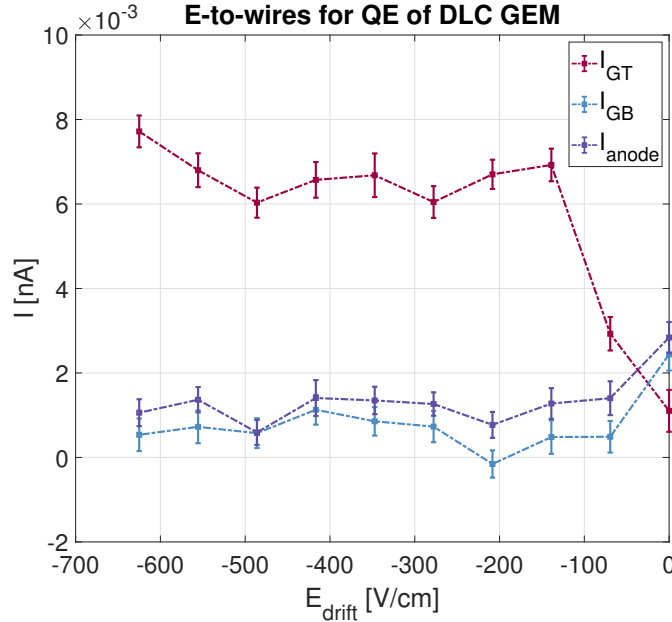


Figure 27: This is the e-to-wires measurement used to determine the number of photoelectrons leaving the DLC GEM. The used filter throughout the QE measurement process is the 171nm-filter.

Figure 27 shows the e-to-wires measurement with the 171nm-filter in vacuum, which is used to calculate the QE of the DLC GEM. At a wavelength of  $\lambda = 161$  nm

the QE of the DLC GEM is  $0.03 \pm 0.02\%$ , which is significantly lower to that of the CsI PC. The QE of the DLC GEM for the visible light range will have to be investigated in future studies.

### 3.4 Aging studies

#### 3.4.1 Exposure to gas

After coating the THGEM #6 with a 205 nm thick CsI layer and installing it into our setup, the detector vessel was flushed with Ar-CH<sub>4</sub> (90-10). Over a period of seven days, e-to-wires measurements with the 171nm-filter were conducted in the morning and evening. The time between the morning and evening measurements was five hours and the time between the evening and morning measurements was 14 hours. The time between measurements and the warm-up phase of the lamp was always the same.

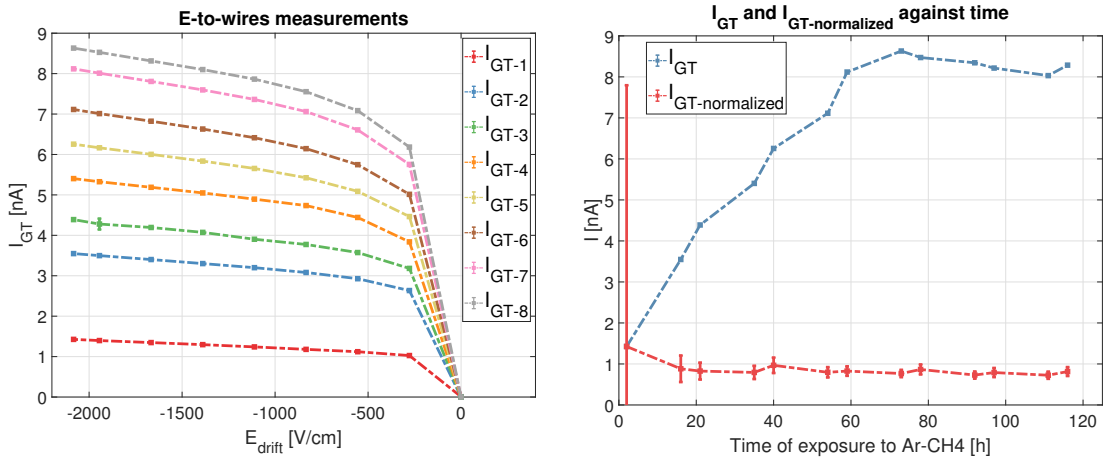


Figure 28: *Left plot:* This shows eight back-to-back e-to-wires measurements in gas and the values of  $I_{GT}$  plotted against the drift field  $E_{drift}$ . *Right plot:* The max. value of  $I_{GT}$  and its normalized value  $I_{GT-normalized}$  plotted against the measurement period of the Aging studies in gas.

The left plot in figure 28 shows the recorded  $I_{GT}$  values against the applied electric field  $E_{drift}$ , which reached values of about  $-2200$  V/cm. The eight different colors indicate the chronological order of the performed measurements. This is at the first glance quite surprising, because the maximum value for  $I_{GT}$  for successive measurements seems to increase, which means the QE of the PC would increase over time in gas. This isn't the case and the reason for the increase in  $I_{GT}$  is connected to the output of the lamp, which increased over the first eight measurements. This can be viewed in the right plot in figure 33 in the appendix.

Because of the unstable output of the lamp, the maximum  $I_{GT}$  of each measurement has to be normalized. The ratio of the  $I_{suck}$  value at the first measurement to the  $I_{suck}$  value for each successive measurement is calculated. Then multiplying this individual value to the maximum  $I_{GT}$  of each measurement yields the normalized current  $I_{GT-normalized}$ , which is plotted on the right in figure 28.

Looking at the plot, one can see that the currents are constant throughout the measurement period when including the uncertainty region. The first value for  $I_{GT-normalized}$  has relatively high uncertainty, due to the big uncertainty in the  $I_{suck}$  value.

In summary, one can say, that exposure to the gas Ar-CH<sub>4</sub> has no impact on the quality of the PC. This is quite important because this means the QE of the CsI, which is calculated from e-to-wires measurement in vacuum (see section 3.3), has not changed from its initial installation into the detector vessel.

It should be mentioned that the effect of photon bombardment on the quality of the PC in gas was not considered nor observed. In vacuum, the photon bombardment results in a photolysis process, where the CsI is split into its ionic components. The iodine then leaves the PC and because the caesium atoms have a high electron affinity the QE of the CsI PC is lowered [31].

In gas, this process seems to be suppressed by the gas molecules. Photon induced aging of PCs in gas appears under intense photon flux ( $\approx 10^{10} [\frac{\text{photons}}{\text{mm}^2 \text{s}}]$ ) and its effects are significantly lower than in vacuum [32]. This is the reason we don't see this aging effect, as each e-to-wires measurement only lasts a relatively short time ( $\approx 1$  h) and the photon flux is only around  $10^8 [\frac{\text{photons}}{\text{mm}^2 \text{s}}]$ .

#### 3.4.2 Ion bombardment

At a potential difference of around  $\Delta U_{THGEM} = 500$  V during gain measurements, electron multiplication in the holes starts occurring. This time the focus is not on the multiplication factor of electrons, but rather on the number of gas ions leaving the hole and hitting the top side of the THGEM. Similar to the case of photon bombardment, the impact of the positive gas ions on the PC results in the dissociation of CsI [31].

Normally we would measure the amount of ions hitting the illuminated area of the PC by recording the positive current on THGEM top  $I_{GT}$  with the pA-meter. But during these gain measurements the current on the THGEM is too high for the safe operation of the pA-meter (current limit 130 nA). Therefore we have to use the Keithley electrometer, which can record these high currents. The problem with using the Keithley electrometer is, that it can only measure the current at electrodes at ground potential. If we were to measure  $I_{GT}$  this would mean having THGEM top grounded. To increase  $\Delta U_{THGEM}$  during gain measurements, the voltage at THGEM bot  $U_{GB}$  would have to be positive and increase. There is a voltage supply (mesytec) in our laboratory that could supply positive voltage to the electrodes, but the voltage range is limited to  $-400$  V to  $400$  V, which would not suffice for this experiment. Ultimately the only other remaining option to calculate the charge per area on the PC is to measure and use the current at THGEM bot  $I_{GB}$ . When recording this current with the Keithley electrometer we can increase  $\Delta U_{THGEM}$  by increasing the voltage at the THGEM top  $U_{GT}$  to high negative values.

But there is a problem when using  $I_{GB}$  for determining the number of ions. Integrating  $I_{GB}$  over the measurement period doesn't directly correspond to the charge deposited onto the PC. Firstly the integration limits have to be adjusted,

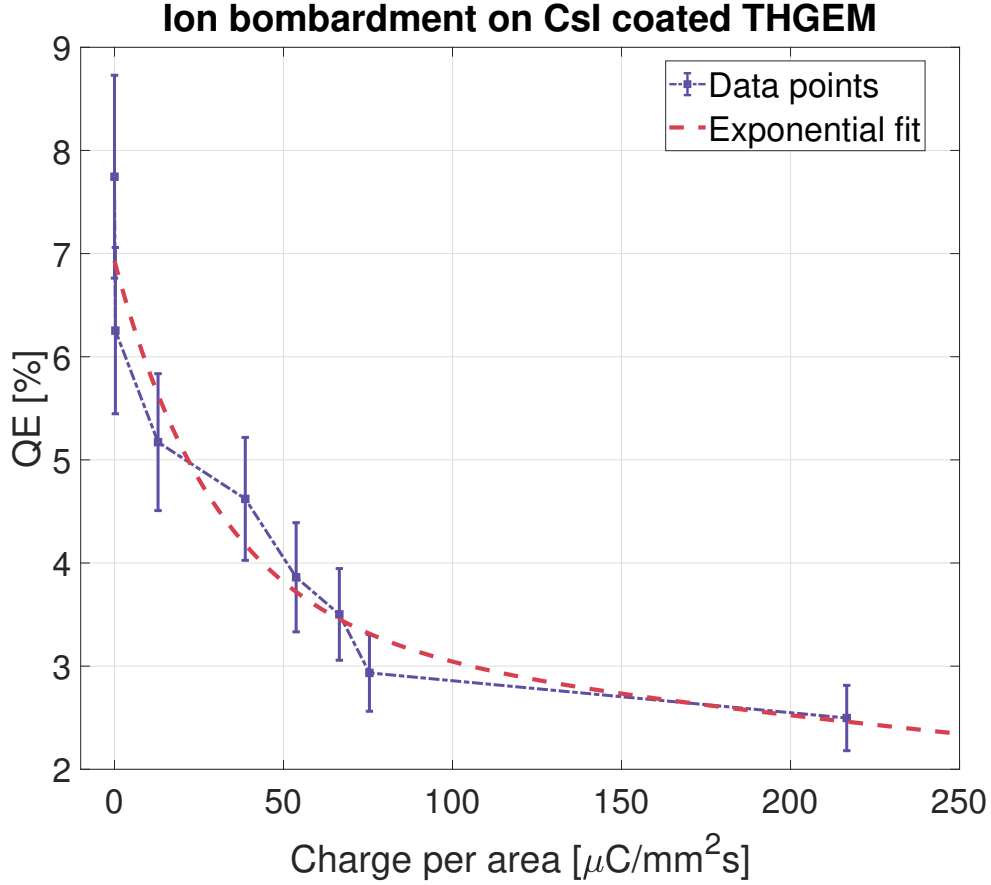


Figure 29: The QE at a wavelength of  $\lambda = 161$  nm of the CsI 205 nm thick coated THGEM plotted against the charge deposited onto the topside of the THGEM.

because electron multiplication and the resulting ion bombarding only starts to happen at a certain  $\Delta U_{THGEM}$ . Therefore the plateau region mentioned in section 3.2 must be determined for each gain measurement.

And because the absolute value  $I_{GB}$  is equal to  $I_{GT}$  during gain measurements, the current  $I_{prim}$  has to be subtracted from  $I_{GB}$ . The reason is, that the positive current  $I_{GT}$  does not only correspond to ions hitting the PC, but also to the emitted photoelectrons leaving the PC. Therefore, to get a value for the charge deposited onto the PC,  $I_{ion} = |I_{GB}| - I_{prim}$  is integrated over the adjusted measurement period. The resulting value then has to be divided by the illuminated area of the PC, which is the coated CsI area beneath the hole of the aperture. We assume that the ion bombardment is uniform across the illuminated area of the PC.

After each gain measurement, the QE of the PC was measured. The process of determining the QE is explained in section 3.3. Ultimately the decrease of QE due to ion bombardment can be seen in figure 29. As one can see, the initial QE value 7.74% drops around 50% at a charge deposition of around  $50 \mu\text{C}/\text{mm}^2\text{s}$ . This trend continues as at a charge deposition of around  $220 \mu\text{C}/\text{mm}^2\text{s}$  on the PC the QE drops to a value of 2.5% for a wavelength of  $\lambda = 161$  nm.

### 3.4 Aging studies

The fit seen in the plot above is the following function

$$f(x) = a \cdot \exp(-b \cdot x) + c \cdot \exp(-d \cdot x),$$

which is the best fit to the raw data and is used by Anderson et al. to model the aging process of the PC [32]. Most of the data points with their uncertainty match the exponential fit. It should be mentioned that the decrease of QE of CsI coated THGEMs due to ion bombardment differ from experiment to experiment and is not well understood [31]. The raw data sets of the current  $I_{GB}$  recorded with the Keithley electrometer during gain measurements and later used for the calculation of the charge can be viewed in figures 36 to 41.

## 4 Summary and outlook

In this thesis, CsI coated THGEMs were characterized. This process started by gaining an understanding of the movement of electrons inside the detector at negative drift fields. The corresponding measurements were performed in gas and vacuum. Thereafter the attainable gain of the single THGEM setup in Ar-CH<sub>4</sub> (90-10) was studied. In order to calculate the gain, a detailed explanation was provided on how to determine the number of initial electrons  $I_{prim}$ . This was done for an uncoated and a CsI coated THGEM. In both cases, a gain of around  $1.2 \cdot 10^3$  was reached before discharges began occurring.

Next, the QE of a CsI coated THGEM was calculated. To achieve this, a diode reference measurement and an e-to-wires measurement in vacuum were performed. The QE of the reflective CsI PC at a wavelength of  $\lambda = 161 \text{ nm}$  was equal to  $7.74 \pm 0.98\%$ . This value could have been even higher if it were possible to treat the coated THGEM with heat after coating it at the facility of the TUM.

Lastly, the aspect of aging of the reflective CsI PC was investigated. This included taking multiple e-to-wires measurements in gas to check if exposure to Ar-CH<sub>4</sub> (90-10) resulted in a decline in the quality of the PC. This was not the case. Another aspect of the aging study was to see how ion bombardment impacted the QE of the PC. This effect was quite detrimental and led to a decrease in quantum efficiency of 50% after a charge deposition of around  $50 \mu\text{C}/\text{mm}^2\text{s}$  on the PC.

The research conducted in this thesis on CsI coated THGEMs has already been performed in more detail by multiple other research groups around the world. Therefore the focus was not on doing research that could improve modern CsI coated THGEM photodetectors, but rather on understanding and verifying the results we obtain with this specific detector setup. Ultimately, the goal is to incorporate reflective PCs into our setup, that have a high QE for the low visible light range, and study the resulting performance. To this day, no THGEM based photodetector for the visible light range has been developed to be used in any large-scale experiments, because there are still many unresolved issues regarding the choice of PC material. To find solutions for these issues, more research has to be conducted, especially as THGEM based photodetectors have the unique potential for large-scale application. Considering that many new detectors have to be scaled up in size in order to make more precise measurements (e.g. Hyper-Kamiokande), the research into THGEM based photodetectors will only intensify in the future.

## List of Figures

1	The inside of the Super-Kamiokande detector, which is surrounded by thousands of photomultiplier tubes. Credit: Jordy Meow [4]. . .	4
2	Dimensions of a standard THGEM.[9] . . . . .	5
3	The electric field in and around a GEM covered with a photosensitive layer is shown in this picture. [11]. . . . .	6
4	This picture illustrates different applications for THGEMs: As an ionizing particle detector or a photodetector with a reflective or a semitransparent PC [13] . . . . .	7
5	This is the detector vessel used during the experiment. These pictures depict the detector in a clean room environment and not in operational mode. . . . .	9
6	This is the operational setup. (1) shows the gas bottle filled with Ar-CH <sub>4</sub> in a 90-10 mixture. (2) shows the Keithley electrometer and (3) the pA-meter. (4) shows the vacuum pump and (5) the high voltage supply. (6) shows the detector vessel and (7) the Cathedon lamp power supply. Lastly (8) shows the FPGA board (Cyclone 4-USB 2.0). . . . .	10
7	This is a sketch of the operational setup. All connections from and to the detector vessel are shown. . . . .	10
8	This sketch shows the cross section of the detector vessel. The Deuterium lamp, the vacuum valve, the filter wheel and the electrodes are depicted. The current measured and voltage supplied at each electrode (1)-(6) is shown. The electric field between each electrode is shown as (7)-(10). The variable names assigned to each number in the figure are documented in table 1. . . . .	11
9	This picture was taken during the coating process. The CsI is heated and evaporated onto sections of the uncoated THGEM. The blue circle in the middle of the picture is the used CsI pill. . . . .	13
10	<i>Left figure:</i> CsI coated THGEM after completion of measurements. The thickness of this CsI PC was 192 nm, which was measured at the clean room coating facility at the TUM. One can see an indication of a circle on the bottom coated area. This was due to this area being illuminated by the lamp, as it was directly beneath the hole of the aperture. <i>Right figure:</i> CsI coated THGEM with cables attached. The THGEM, sectioned in three segments, had two parts coated with CsI. . . . .	14
11	<i>Left picture:</i> The wavelength spectrum of the used Deuterium lamp. The relative intensity is highest for wavelengths around $\lambda = 161$ nm due to the built-in MgF <sub>2</sub> window [20]. The energy of the emitted photons range from $E_{\text{photon}} = 5.64 - 10.78$ eV. <i>Right picture:</i> The output of the lamp is folded with the transmission of the 171nm-filter. . . . .	16

List of Figures

12	<p><i>Left picture:</i> The spectral response of the diode, used for reference measurements to determine the QE of the CsI coating.[21]. <i>Right picture:</i> This picture shows an example of the Diode measurement. The diode is placed in the middle of the hole in this picture. . . . .</p>	17
13	<p>This picture highlights the movement of the emitted photoelectrons during the e-to-wires measurement. The electric field <math>E_{drift}</math> is negative so that electrons emitted from the PC get accelerated to the wires. . . . .</p>	18
14	<p>Currents at each electrode plotted against the drift field <math>E_{drift}</math>. The filter <math>\text{CaF}_2</math> and the CsI 195 nm thick coated THGEM were used. . .</p>	20
15	<p>This plot shows the low drift field region recorded during the e-to-wires measurement in vacuum. The filter <math>\text{CaF}_2</math> and the CsI 195 nm thick coated THGEM were used. . . . .</p>	21
16	<p>Currents measured at each electrode plotted against the drift field <math>E_{drift}</math>. The filter <math>\text{CaF}_2</math> and the CsI 195 nm thick coated THGEM were used. . . . .</p>	24
17	<p><i>Left plot:</i> An <math>E_{drift}</math> scan at <math>\Delta U_{THGEM} = 600</math> V. <i>Right plot:</i> An <math>E_{drift}</math> scan at <math>\Delta U_{THGEM} = 800</math> V. These measurements were performed with the CsI 195 nm thick coated THGEM and the <math>\text{CaF}_2</math> filter in <math>\text{Ar}-\text{CH}_4</math> (90-10). . . . .</p>	25
18	<p>The measured currents plotted against the <math>E_{drift}</math>. The current <math>I_{suck}</math> is not shown, as it would distort the graph. The 171nm-filter and CsI 205 nm thick coated THGEM in vacuum was used. . . . .</p>	27
19	<p>The measured currents plotted against the <math>\Delta U_{THGEM}</math> at the THGEM. The 171nm-filter and CsI 205 nm thick coated THGEM in vacuum was used. . . . .</p>	27
20	<p>The electron movement during an e-through-hole measurement. There is no electron multiplication because this measurement is performed in vacuum. . . . .</p>	28
21	<p><i>Left plot:</i> The absolute value of <math>I_{GB}</math> plotted half logarithmic against the potential difference <math>\Delta U_{THGEM}</math>. The uncertainties are left out but can be viewed in figure 35. <i>Right plot:</i> The e-to-wires measurement in <math>\text{Ar}-\text{CH}_4</math> (90-10). Both measurements are performed with the CsI 205 nm thick coated THGEM and the 171nm-filter. . . . .</p>	29
22	<p><i>Left plot:</i> The absolute value of <math>I_{GB}</math> plotted half logarithmic against the potential difference <math>\Delta U_{THGEM}</math>. The uncertainties are left out but can be viewed in figure 35. <i>Right plot:</i> The e-to-wires measurement in <math>\text{Ar}-\text{CH}_4</math> (90-10). Both measurements are done with uncoated Au THGEM #5 and the <math>\text{SiO}_2</math> filter. . . . .</p>	30
23	<p>Gain of CsI 205 nm thick coated THGEM. The 171nm-filter was used. . . . .</p>	30
24	<p>Gain of uncoated Au THGEM. The <math>\text{SiO}_2</math> filter was used. . . . .</p>	31
25	<p>This is the e-to-wires measurement used to determine the number of photoelectrons leaving the CsI PC. This measurement was done in vacuum and with the 171nm-filter. . . . .</p>	32

List of Figures

26	This plot shows the currents measured at each diode position. The used filter throughout the QE measurement process is the 171nm-filter. . . . .	33
27	This is the e-to-wires measurement used to determine the number of photoelectrons leaving the DLC GEM. The used filter throughout the QE measurement process is the 171nm-filter. . . . .	34
28	<i>Left plot:</i> This shows eight back-to-back e-to-wires measurements in gas and the values of $I_{GT}$ plotted against the drift field $E_{drift}$ . <i>Right plot:</i> The max. value of $I_{GT}$ and its normalized value $I_{GT-normalized}$ plotted against the measurement period of the Aging studies in gas. . . . .	35
29	The QE at a wavelength of $\lambda = 161$ nm of the CsI 205 nm thick coated THGEM plotted against the charge deposited onto the topside of the THGEM. . . . .	37
30	The transmission of the 171nm-filter plotted against the wavelength. It has a transmission of 17.5% at $\lambda = 171$ nm and $\sigma = 20$ nm. . . . .	44
31	This picture depicts an exemplary uncoated Au THGEM (# 1). . . . .	44
32	The output of the lamp varied from day to day operation during the diode reference measurements. The current measured at each diode location had to be adjusted. . . . .	45
33	<i>Left plot:</i> The current of the aperture $I_{suck}$ is plotted the voltage at the aperture $U_{aperture}$ . <i>Right plot:</i> The output of the lamp, measured indirectly through $I_{suck}$ , is not constant over the measurement period of the aging studies in gas. . . . .	45
34	Comparison of e to wires measurement with $U_{GT} = U_{GB} = -500$ V and $U_{GT} = U_{GB} = 0$ V. The uncertainty for the $-500$ V case is in the order of $10^{-3}$ and for the $0$ V case in the order of $10^{-4}$ . . . . .	46
35	<i>Left plot:</i> The absolute value of $I_{GB}$ plotted against $\Delta U_{THGEM}$ for the case of the uncoated THGEM. <i>Right plot:</i> The absolute value of $I_{GB}$ plotted against $\Delta U_{THGEM}$ for the case of the coated THGEM. . . . .	46
36	Second gain measurement performed with Keithley eletrometer. The excluded points are not taken into the charge per area calculation. The excluded area on the left is at values of $\Delta U_{THGEM}$ where the electrons don't have enough energy to ionize gas atoms. The excluded points on the right are recorded discharges, where the values of the recorded current peak. This exclusion principle is the same for all following figures. During the first gain measurement the Keithley did not work. Therefore the pA-meter had to be used and $\Delta U_{THGEM}$ was increased, until a current of $I = 130$ nA. The charge per area for the first measurement is way lower compared to gain measurements with the Keithley electrometer and is $0.268\mu C/mm^2s$ . . . . .	47
37	Third gain measurement performed with Keithley eletrometer. . . . .	47
38	Fourth gain measurement performed with Keithley eletrometer. . . . .	47
39	Fifth gain measurement performed with Keithley eletrometer. . . . .	48
40	Sixth gain measurement performed with Keithley eletrometer. . . . .	48
41	Seventh gain measurement performed with Keithley eletrometer. . . . .	48

## List of Tables

1	<i>Left table:</i> This table documents the variable name, the measured currents and the supplied voltage of each electrode. <i>Right table:</i> This table documents the variable names of the electric field between the respective electrodes and indicates between which electrode which electric field exists. All numbers are in accordance to the sketch in figure 8. . . . .	12
2	Work functions of electrode material. The work functions depend heavily on gas and preparation, but these values should give an indication if photo electrons can be emitted by photons of the UV-lamp.[15] [16] . . . . .	12
3	The distance $d$ between the individual electrodes is shown. . . . .	12
4	This table documents the used filters and the wavelengths that can pass through the individual filter. . . . .	44
5	This table documents the measured leakage currents of the THGEMs used during these experiments. . . . .	44

## 5 Appendix

Table 4: This table documents the used filters and the wavelengths that can pass through the individual filter.

filters	wavelength [nm]
SiO <sub>2</sub>	> 185
CaF <sub>2</sub>	> 180
171nm	161

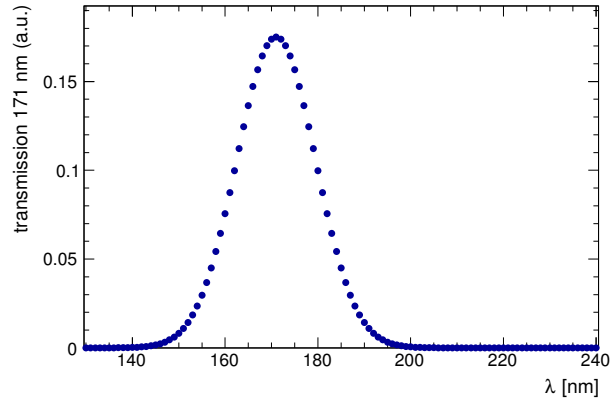


Figure 30: The transmission of the 171nm-filter plotted against the wavelength. It has a transmission of 17.5% at  $\lambda = 171$  nm and  $\sigma = 20$ nm.

THGEMs #	sector	leakage current [nA]
3	a	16
	b	6
	c	7
5	a	8
	b	6
	c	7
6	a	7
	b	7
	c	7

Table 5: This table documents the measured leakage currents of the THGEMs used during these experiments.

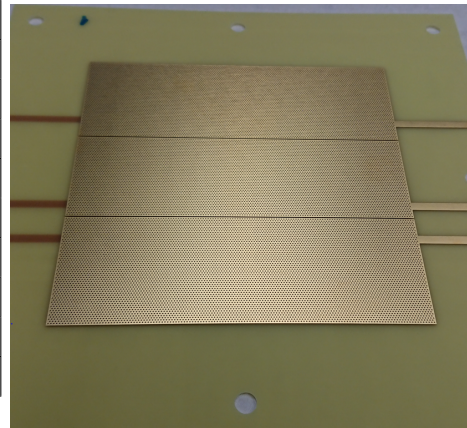


Figure 31: This picture depicts an exemplary uncoated Au THGEM (# 1).

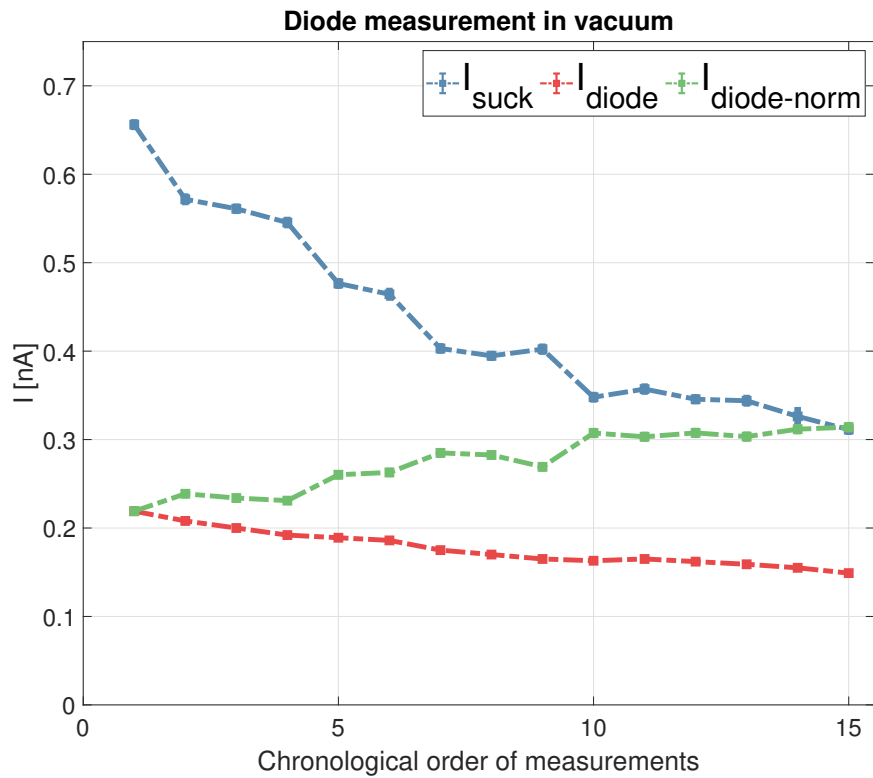


Figure 32: The output of the lamp varied from day to day operation during the diode reference measurements. The current measured at each diode location had to be adjusted.

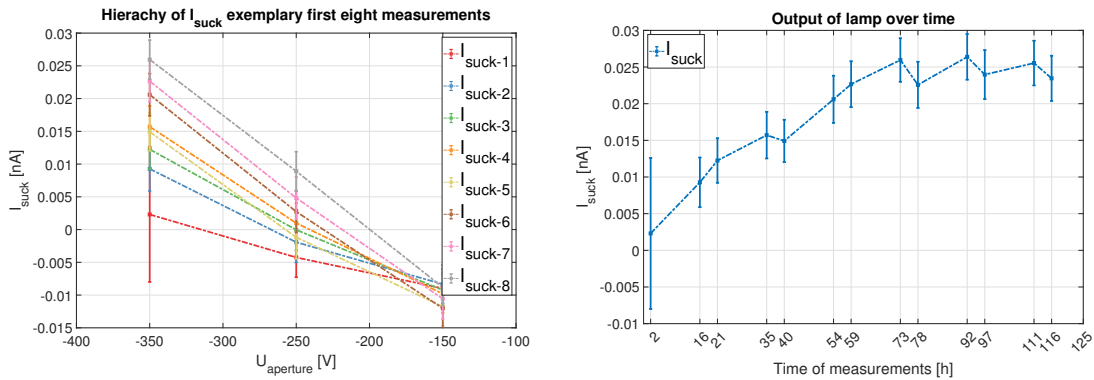


Figure 33: *Left plot:* The current of the aperture  $I_{suck}$  is plotted the voltage at the aperture  $U_{aperture}$ . *Right plot:* The output of the lamp, measured indirectly through  $I_{suck}$ , is not constant over the measurement period of the aging studies in gas.

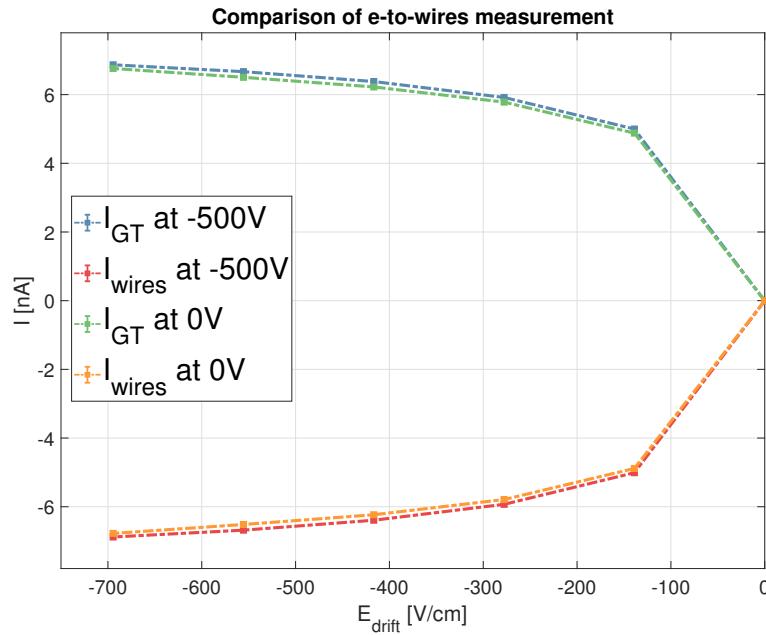


Figure 34: Comparison of e to wires measurement with  $U_{GT} = U_{GB} = -500$  V and  $U_{GT} = U_{GB} = 0$  V. The uncertainty for the  $-500$  V case is in the order of  $10^{-3}$  and for the  $0$  V case in the order of  $10^{-4}$ .

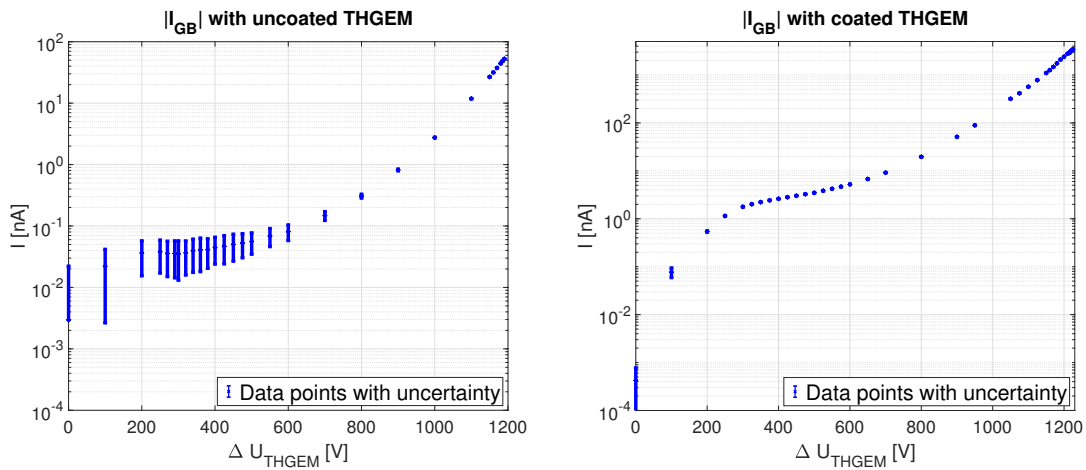


Figure 35: *Left plot:* The absolute value of  $I_{GB}$  plotted against  $\Delta U_{THGEM}$  for the case of the uncoated THGEM. *Right plot:* The absolute value of  $I_{GB}$  plotted against  $\Delta U_{THGEM}$  for the case of the coated THGEM.

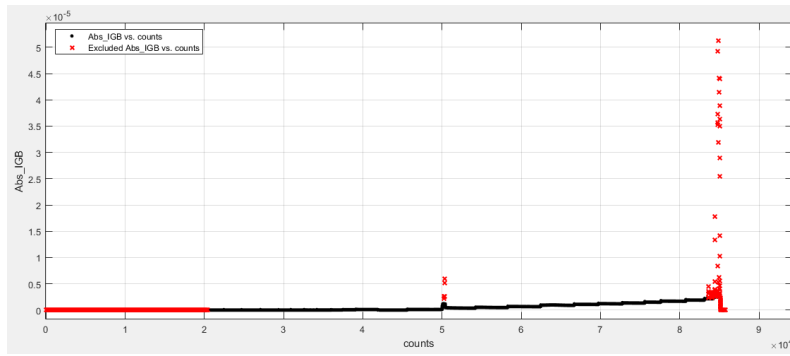


Figure 36: Second gain measurement performed with Keithley eletrometer. The excluded points are not taken into the charge per area calculation. The excluded area on the left is at values of  $\Delta U_{THGEM}$  where the electrons don't have enough energy to ionize gas atoms. The excluded points on the right are recorded discharges, where the values of the recorded current peak. This exclusion principle is the same for all following figures. During the first gain measurement the Keithley did not work. Therefore the pA-meter had to be used and  $\Delta U_{THGEM}$  was increased, until a current of  $I = 130 \text{ nA}$ . The charge per area for the first measurement is way lower compared to gain measurements with the Keithley eletrometer and is  $0.268 \mu\text{C}/\text{mm}^2\text{s}$ .

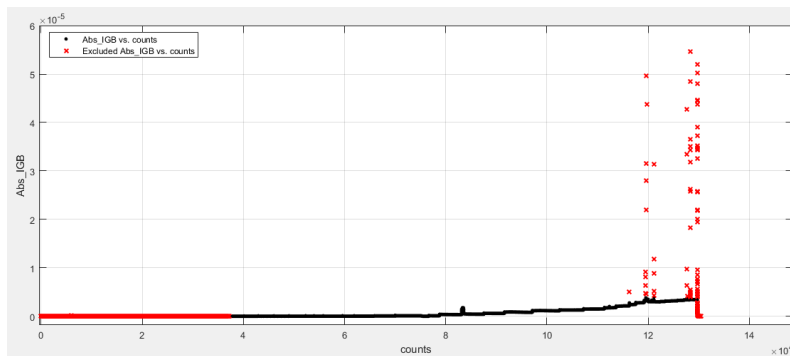


Figure 37: Third gain measurement performed with Keithley eletrometer.

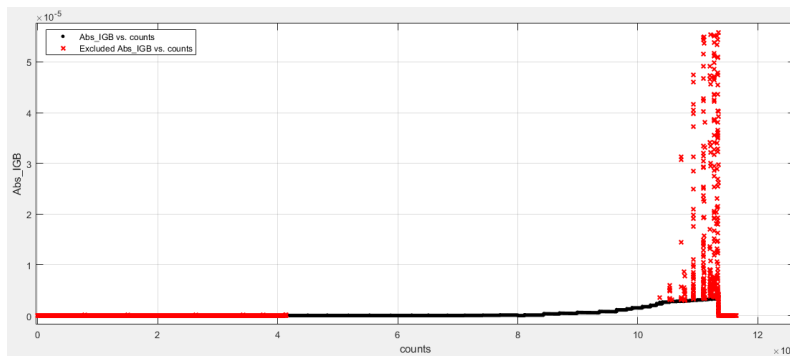


Figure 38: Fourth gain measurement performed with Keithley eletrometer.

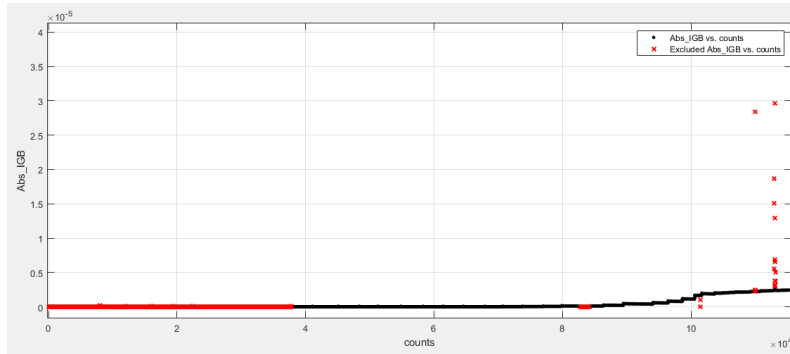


Figure 39: Fifth gain measurement performed with Keithley electrometer.

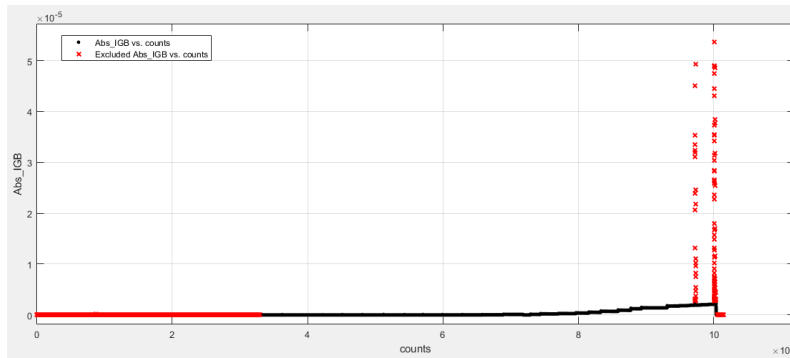


Figure 40: Sixth gain measurement performed with Keithley electrometer.

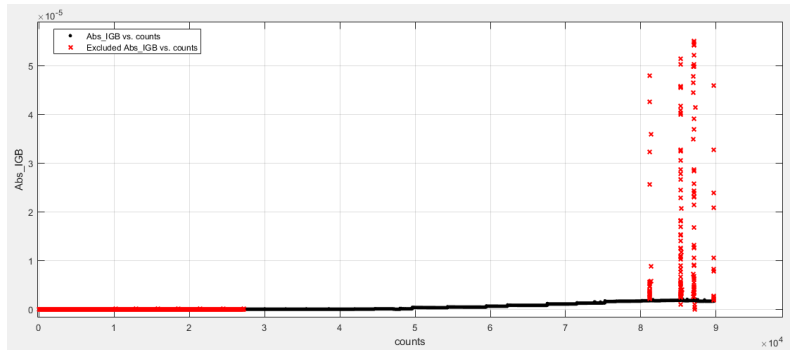


Figure 41: Seventh gain measurement performed with Keithley electrometer.

## 6 Acknowledgements

First and foremost, I would like to express my gratitude to my supervisor Thomas Klemenz. You always gave me helpful advice and never seemed to be annoyed by my constant and sometimes redundant questions. Next, I want to thank Dr. Piotr Gasik for his helpful advice and his immense expertise regarding THGEMs. Another huge thanks goes to Berkin Ulukutlu and Henrik Friert for the friendly company and their useful input during the weekly meetings. I also want to thank Prof. Laura Fabbietti for giving me the opportunity to conduct research and be a part of her very friendly group. Another big thanks goes to Dr. Roman Gernhäuser who helped us coat the THGEMs and asked very interesting and helpful questions. Lastly, I would like to thank my friends and family for always supporting me.

## References

- [1] F. Reines and C. L. Cowan. “Detection of the Free Neutrino.” In: *Phys. Rev.* 92 (3 Nov. 1953), pp. 830–831. DOI: [10.1103/PhysRev.92.830](https://doi.org/10.1103/PhysRev.92.830). URL: <https://link.aps.org/doi/10.1103/PhysRev.92.830>.
- [2] Y. Fukuda et al. “Evidence for Oscillation of Atmospheric Neutrinos.” In: *Phys. Rev. Lett.* 81 (8 Aug. 1998), pp. 1562–1567. DOI: [10.1103/PhysRevLett.81.1562](https://doi.org/10.1103/PhysRevLett.81.1562). URL: <https://link.aps.org/doi/10.1103/PhysRevLett.81.1562>.
- [3] and Mark Aartsen et al. “Neutrino emission from the direction of the blazar TXS 0506+056 prior to the IceCube-170922A alert.” In: *Science* 361.6398 (July 2018), pp. 147–151. DOI: [10.1126/science.aat2890](https://doi.org/10.1126/science.aat2890). URL: <https://doi.org/10.1126%2Fscience.aat2890>.
- [4] *Super-Kamiokande: The Neutrino Detector*. Last visited on 21.08.2022. offbeat-japan.org. URL: <https://offbeatjapan.org/super-kamiokande-neutrino-detector/>.
- [5] *Photomultiplier Tubes*. Last visited on 17.08.2022. Hamamatsu. URL: [https://www.hamamatsu.com/content/dam/hamamatsu-photonics/sites/documents/99\\_SALES\\_LIBRARY/etd/PMT\\_handbook\\_v3aE.pdf](https://www.hamamatsu.com/content/dam/hamamatsu-photonics/sites/documents/99_SALES_LIBRARY/etd/PMT_handbook_v3aE.pdf).
- [6] S. Fukuda et al. “The Super-Kamiokande detector.” In: *Nuclear Instruments and Methods in Physics Research Section A: Accelerators, Spectrometers, Detectors and Associated Equipment* 501.2 (2003), pp. 418–462. ISSN: 0168-9002. DOI: [https://doi.org/10.1016/S0168-9002\(03\)00425-X](https://doi.org/10.1016/S0168-9002(03)00425-X). URL: <https://www.sciencedirect.com/science/article/pii/S016890020300425X>.
- [7] F. Sauli. “GEM: A new concept for electron amplification in gas detectors.” In: *Nuclear Instruments and Methods in Physics Research Section A: Accelerators, Spectrometers, Detectors and Associated Equipment* 386.2 (1997), pp. 531–534. ISSN: 0168-9002. DOI: [https://doi.org/10.1016/S0168-9002\(96\)01172-2](https://doi.org/10.1016/S0168-9002(96)01172-2). URL: <https://www.sciencedirect.com/science/article/pii/S0168900296011722>.
- [8] *How to get GEMs*. Last visited on 04.08.2022. Gas Detector Development Group. URL: <https://gdd.web.cern.ch/gem-gettinggems>.
- [9] A. Breskin et al. “A concise review on THGEM detectors.” In: *Nuclear Instruments and Methods in Physics Research Section A: Accelerators, Spectrometers, Detectors and Associated Equipment* 598.1 (2009). Instrumentation for Colliding Beam Physics, pp. 107–111. ISSN: 0168-9002. DOI: <https://doi.org/10.1016/j.nima.2008.08.062>. URL: <https://www.sciencedirect.com/science/article/pii/S0168900208012047>.
- [10] R. Chechik, A. Breskin, and C. Shalem. “Thick GEM-like multipliers—a simple solution for large area UV-RICH detectors.” In: *Nuclear Instruments and Methods in Physics Research Section A: Accelerators, Spectrometers, Detectors and Associated Equipment* 553.1 (2005). Proceedings of the fifth International Workshop on Ring Imaging Detectors, pp. 35–40. ISSN: 0168-9002. DOI: [https://doi.org/10.1016/S0168-9002\(05\)00000-0](https://doi.org/10.1016/S0168-9002(05)00000-0).

## References

- [//doi.org/10.1016/j.nima.2005.08.003](https://doi.org/10.1016/j.nima.2005.08.003). URL: <https://www.sciencedirect.com/science/article/pii/S0168900205015664>.
- [11] A. F. Buzulutskov. “Gaseous photodetectors with solid photocathodes.” In: *Physics of Particles and Nuclei* 39.3 (June 2008), p. 424. ISSN: 1531-8559. DOI: [10.1134/S1063779608030052](https://doi.org/10.1134/S1063779608030052). URL: <https://doi.org/10.1134/S1063779608030052>.
- [12] A. B. Arons and M. B. Peppard. “Einstein’s Proposal of the Photon Concept—a Translation of the Annalen der Physik Paper of 1905.” In: *American Journal of Physics* 33.5 (1965), pp. 367–374. DOI: [10.1119/1.1971542](https://doi.org/10.1119/1.1971542). eprint: <https://doi.org/10.1119/1.1971542>. URL: <https://doi.org/10.1119/1.1971542>.
- [13] C. Shalem et al. “Advances in Thick GEM-like gaseous electron multipliers—Part I: atmospheric pressure operation.” In: *Nuclear Instruments and Methods in Physics Research Section A: Accelerators, Spectrometers, Detectors and Associated Equipment* 558.2 (2006), pp. 475–489. ISSN: 0168-9002. DOI: <https://doi.org/10.1016/j.nima.2005.12.241>. URL: <https://www.sciencedirect.com/science/article/pii/S016890020502680X>.
- [14] K. Zeitelhack et al. “The HADES RICH detector.” In: *Nuclear Instruments and Methods in Physics Research Section A: Accelerators, Spectrometers, Detectors and Associated Equipment* 433.1 (1999), pp. 201–206. ISSN: 0168-9002. DOI: [https://doi.org/10.1016/S0168-9002\(99\)00371-X](https://doi.org/10.1016/S0168-9002(99)00371-X). URL: <https://www.sciencedirect.com/science/article/pii/S016890029900371X>.
- [15] *Common Work Functions*. Last visited on 03.08.2022. <https://www.pulsedpower.net/>. URL: <https://www.pulsedpower.net/Info/workfunctions.htm>.
- [16] Gregory N. Derry, Megan E. Kern, and Eli H. Worth. “Recommended values of clean metal surface work functions.” In: *Journal of Vacuum Science & Technology A* 33.6 (2015), p. 060801. DOI: [10.1116/1.4934685](https://doi.org/10.1116/1.4934685). eprint: <https://doi.org/10.1116/1.4934685>. URL: <https://doi.org/10.1116/1.4934685>.
- [17] J. Friese et al. “Enhanced quantum efficiency for CsI grown on a graphite-based substrate coating.” In: *Nuclear Instruments and Methods in Physics Research Section A: Accelerators, Spectrometers, Detectors and Associated Equipment* 438.1 (1999), pp. 86–93. ISSN: 0168-9002. DOI: [https://doi.org/10.1016/S0168-9002\(99\)00663-4](https://doi.org/10.1016/S0168-9002(99)00663-4). URL: <https://www.sciencedirect.com/science/article/pii/S0168900299006634>.
- [18] C. Lu and K.T. McDonald. “Properties of reflective and semitransparent CsI photocathodes.” In: *Nuclear Instruments and Methods in Physics Research Section A: Accelerators, Spectrometers, Detectors and Associated Equipment* 343.1 (1994), pp. 135–151. ISSN: 0168-9002. DOI: [https://doi.org/10.1016/0168-9002\(94\)90543-6](https://doi.org/10.1016/0168-9002(94)90543-6). URL: <https://www.sciencedirect.com/science/article/pii/0168900294905436>.

- [19] E Schyns. "Status of large area CsI photocathode developments." In: *Nuclear Instruments and Methods in Physics Research Section A: Accelerators, Spectrometers, Detectors and Associated Equipment* 494.1 (2002). Proceedings of the 8th International Conference on Instrumentation for Colliding Beam Physics, pp. 441–446. ISSN: 0168-9002. DOI: [https://doi.org/10.1016/S0168-9002\(02\)01520-6](https://doi.org/10.1016/S0168-9002(02)01520-6). URL: <https://www.sciencedirect.com/science/article/pii/S0168900202015206>.
- [20] *Deuterium lamps*. Last visited on 21.08.2022. URL: [https://www.hamamatsu.com/content/dam/hamamatsu-photonics/sites/documents/99\\_SALES\\_LIBRARY/etd/D2lamps\\_TLS1017E.pdf](https://www.hamamatsu.com/content/dam/hamamatsu-photonics/sites/documents/99_SALES_LIBRARY/etd/D2lamps_TLS1017E.pdf).
- [21] *GaP Photodiode FGAP71*. Last visited on 30.07.2022. thorlabs.de. URL: <https://www.thorlabs.de/drawings/fb7896eff4684140-0C8CF264-973D-DBA7-48AE4577895DE279/FGAP71-SpecSheet.PDF>.
- [22] *Hinweise zur Beurteilung von Messungen, Messergebnissen und Messunsicherheiten (ABW)*. Last visited on 06.08.2022. Technical University of Munich. URL: <https://www.ph.tum.de/academics/org/labs/ap/org/ABW.pdf>.
- [23] E. Aprile et al. "Electron extraction from a CsI photocathode into condensed Xe, Kr, and Ar." In: *Nuclear Instruments and Methods in Physics Research Section A: Accelerators, Spectrometers, Detectors and Associated Equipment* 343.1 (1994), pp. 129–134. ISSN: 0168-9002. DOI: [https://doi.org/10.1016/0168-9002\(94\)90542-8](https://doi.org/10.1016/0168-9002(94)90542-8). URL: <https://www.sciencedirect.com/science/article/pii/0168900294905428>.
- [24] S. Ramo. "Currents Induced by Electron Motion." In: *Proceedings of the IRE* 27.9 (1939), pp. 584–585. DOI: [10.1109/JRPROC.1939.228757](https://doi.org/10.1109/JRPROC.1939.228757).
- [25] A. Buzulutskov, A. Breskin, and R. Chechik. "Field enhancement of the photoelectric and secondary electron emission from CsI." In: *Journal of Applied Physics* 77.5 (1995), pp. 2138–2145. DOI: [10.1063/1.358791](https://doi.org/10.1063/1.358791). eprint: <https://doi.org/10.1063/1.358791>. URL: <https://doi.org/10.1063/1.358791>.
- [26] J Frangenheim. "Measurements of the drift velocity using a small gas chamber for monitoring of the CMS muon system." presented June 2007. 2007. URL: <https://cds.cern.ch/record/2284022>.
- [27] A. Buzulutskov et al. "GEM operation in pure noble gases and the avalanche confinement." In: *Nuclear Instruments and Methods in Physics Research Section A: Accelerators, Spectrometers, Detectors and Associated Equipment* 433.1 (1999), pp. 471–475. ISSN: 0168-9002. DOI: [https://doi.org/10.1016/S0168-9002\(99\)00295-8](https://doi.org/10.1016/S0168-9002(99)00295-8). URL: <https://www.sciencedirect.com/science/article/pii/S0168900299002958>.
- [28] A. Breskin et al. "Field-dependent photoelectron extraction from CsI in different gases." In: *Nuclear Instruments and Methods in Physics Research Section A: Accelerators, Spectrometers, Detectors and Associated Equipment* 367.1 (1995). Proceedings of the 7th International Wire Chamber Conference, pp. 342–346. ISSN: 0168-9002. DOI: [https://doi.org/10.1016/0168-9002\(95\)00295-8](https://doi.org/10.1016/0168-9002(95)00295-8).

## References

- 00639-7. URL: <https://www.sciencedirect.com/science/article/pii/S0168900295006397>.
- [29] M. Alexeev et al. "Progress towards a THGEM-based detector of single photons." In: *Nuclear Instruments and Methods in Physics Research Section A: Accelerators, Spectrometers, Detectors and Associated Equipment* 639.1 (2011). Proceedings of the Seventh International Workshop on Ring Imaging Cherenkov Detectors, pp. 130–133. ISSN: 0168-9002. DOI: <https://doi.org/10.1016/j.nima.2010.10.117>. URL: <https://www.sciencedirect.com/science/article/pii/S0168900210024022>.
- [30] Fabio Sauli. "Gas detectors: Recent developments and future perspectives." In: *Nuclear Instruments and Methods in Physics Research Section A: Accelerators, Spectrometers, Detectors and Associated Equipment* 419.2 (1998), pp. 189–201. ISSN: 0168-9002. DOI: [https://doi.org/10.1016/S0168-9002\(98\)00793-1](https://doi.org/10.1016/S0168-9002(98)00793-1). URL: <https://www.sciencedirect.com/science/article/pii/S0168900298007931>.
- [31] A Breskin. "CsI UV photocathodes: history and mystery." In: *Nuclear Instruments and Methods in Physics Research Section A: Accelerators, Spectrometers, Detectors and Associated Equipment* 371.1 (1996). Proceedings of the Second International Workshop on Ring Imaging Cherenkov Detectors, pp. 116–136. ISSN: 0168-9002. DOI: [https://doi.org/10.1016/0168-9002\(95\)01145-5](https://doi.org/10.1016/0168-9002(95)01145-5). URL: <https://www.sciencedirect.com/science/article/pii/S0168900295011455>.
- [32] D.F. Anderson et al. "Properties of CsI and CsI-TMAE photocathodes." In: *Nuclear Instruments and Methods in Physics Research Section A: Accelerators, Spectrometers, Detectors and Associated Equipment* 323.3 (1992), pp. 626–634. ISSN: 0168-9002. DOI: [https://doi.org/10.1016/0168-9002\(92\)90007-Q](https://doi.org/10.1016/0168-9002(92)90007-Q). URL: <https://www.sciencedirect.com/science/article/pii/S016890029290007Q>.